Manuscript
Click here to view linked References

Title: Coastal inundation under concurrent mean and extreme sea-level rise in Coral Gables, Florida, USA

Authors:

Vladimir J. Alarcon[1]

Anna C. Linhoss[2]

Christopher R. Kelble[3]

Paul F. Mickle[4]

Gonzalo F. Sanchez-Banda[1]

Fernando E. Mardonez-Meza[1]

Joseph Bishop[3]

Steven L. Ashby[4]

Affiliations

(1) Civil Engineering Department, Universidad Diego Portales, Santiago, Chile. vladimir.alarcon@udp.cl, gonzalo.sanchezb@mail.udp.cl, fernando.mardonez@mail.udp.cl

(2) Department of Biosystems Engineering, Auburn University, 3101 Shelby Center Auburn, AL 36849. alinhoss@abe.msstate.edu

(3) Ocean Chemistry & Ecosystems Division, NOAA Atlantic Oceanographic and Meteorological Laboratory, 4301 Rickenbacker Causeway, Miami, FL 33149, chris.kelble@noaa.gov , joe.bishop@noaa.gov

(4) Northern Gulf Institute, Mississippi State University, 2 Research Blvd., Starkville MS pmickle@ngi.msstate.edu

Abstract

Southeast Florida (SF) is among the most vulnerable regions to sea-level rise in the United States of America. The consequences associated with sea-level rise (SLR) are already apparent, including coastal inundation and erosion. The Coral Gables Canal watershed is located in SF and can be considered representative of the effects of combined mean and extreme SLR. In this research, the effect of concurrent mean and extreme sea-level rise on coastal inundation in the Coral Gables Canal watershed is explored. A three-dimensional hydrodynamic model for Biscayne Bay and the Coral Gables Canal is presented. The model is used to estimate water surface elevations throughout the model domain, and map inundation due to an extreme water-level event (Irma Hurricane) occurring alongside mean SLR scenarios. A comparison of the inundation coverage calculated in this research to estimations made by several online tools shows that the online simulators underestimate flooding areas by 72% to 85%. This is a consequence of underpredicting maximum water surface elevations occurring under combined SLR in the Coral Gables Canal. The model predicts that under the NOAA Intermediate High SLR scenario (year 2100), 40% of the CGC watershed will be inundated (water depths > 0.6 m), and 70% of the area will be flooded with water depths greater than 1.6 m in year 2120. Under the NOAA High SLR scenario at least 70% of the Coral Gables Canal watershed would be inundated in 2100 (water depths > 1.0 m). In year 2120, 90% of inland sub-basins will be flooded (0.6 m < depths < 2.2 m). These results are significant for planning flooding/inundation risk management strategies.

Keywords: Coral Gables Canal, coastal inundation, sea-level rise, Irma Hurricane, EFDC

1. Introduction

Global warming, in response to the accumulation of anthropogenically produced greenhouse gases inside the atmosphere, has increased Earth's mean temperature and ocean heat content. This is resulting in glacier and ice sheet melt, and consequently causing global sea level rise (Cazenave and Le Cozannet, 2014; Slangen et al., 2016; Jevrejeva et al., 2009; Gornitz et al., 1997). The potential impact of sea-level rise on coastal zones has become a question of growing interest to the public, because of the far reaching social and economic consequences (Pednekar and Siva Raju, 2020). In the United States of America (US), sea-level rise in the mid-Atlantic coast is twice the global average and exceeds that of the rest of the conterminous US coast, with the exception of coastal Louisiana (Sallenger et al., 2012). Specially in Florida, the impacts of climate change and sea-level rise include flooding, increase in invasive species, damage to the coral reefs, and increased numbers of damaging hurricanes (Palm and Bolsen, 2020).

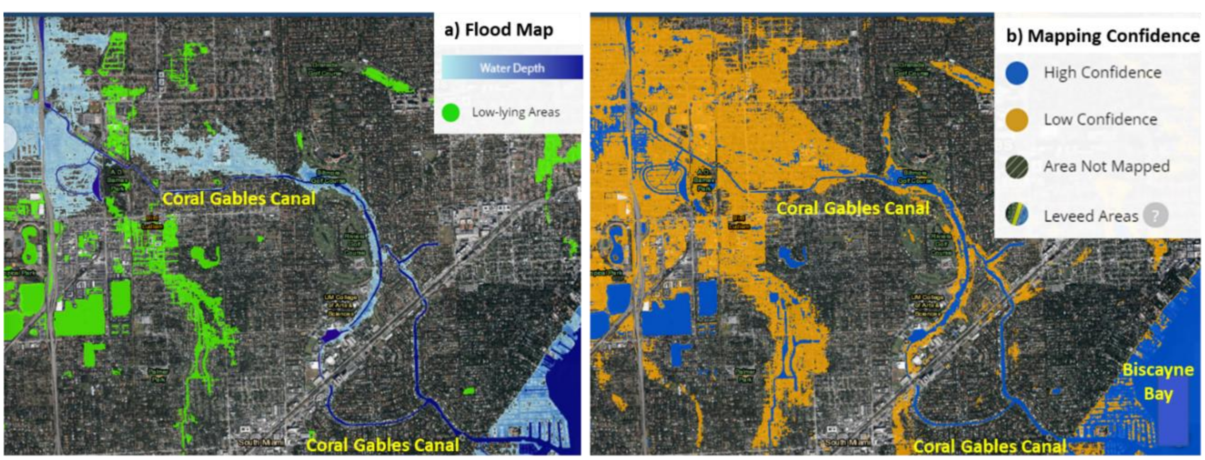

Figure 1. Flooding in the Coral Gables Canal area. 1a) Flood map generated by NOAA's Sea-level Rise Viewer. 1b) Mapping confidence of the projected flood map.

Southeast Florida is among the most vulnerable regions to sea-level rise in the United States, due to the co-occurrence of multiple drivers such as numerous water control structures, rainfall intensity and duration, groundwater level, and ocean-side water level (Jane et al., 2020). The consequences associated with sea-level rise are already apparent, including coastal inundation and erosion, increased frequency of flooding, reduced soil infiltration capacity, saltwater intrusion of drinking-water supply, increased pollution and contamination, and impairment of infrastructure such as roads and septic systems (SFRCCC, 2020). Also, the natural environment is under immediate and real threat. With higher and accelerating sea-level rise today, enhanced climate variability could further hasten the loss of mangrove-lined coastlines, compounded by changes in surface runoff and flow caused by landcover change and unsustainable water management (Wingard, 2021; Jones et al., 2019). Socio-economic impacts such as displacement, decreases in property values and tax base, and increases in insurance costs (SFRCCC, 2020) are producing discounts in pricing of residential properties that are located in flood prone areas (Fu and Nijman, 2021).

The Coral Gables Canal is located in the Biscayne Bay Drainage Basin (Southeast Florida). It can be considered a case study in sea-level rise for the larger, southeast Florida because of its residential and commercial land use, low topography, karst geology, and water control structures regulating outflows. SFRCCC (2020) presented a regionally unified sea-level rise projection, for ensuring consistency in adaptation planning and policy for the Southeast Florida four-county region. This unified sea-level rise projection is based on projections from the National Oceanic and Atmospheric Administration (NOAA) (Sweet et al., 2017). NOAA’s Sea-level Rise Viewer (NOAA, 2017a) allows the generation of inundation maps that illustrate the scale of potential flooding, in water depths relative to Mean Higher High Water (MHHW). Figure 1a) shows the inland extent and relative depth of inundation above MHHW corresponding to year 2100, for the area surrounding the Coral Gables Canal, based on the local scenario at Virginia Key NOAA station. Figure 1b) shows the mapping confidence of the projected flood map. Blue areas denote a high confidence of inundation (confidence ≥ 80%), orange areas denote a low confidence of inundation (confidence < 80%), and unshaded areas denote a high confidence that these areas will be dry (NOAA, 2017a).

The confidence map shown in Figure 1b spatially represents the summation of 1) the uncertainty in the lidar-derived elevation data, and 2) the uncertainty in the modeled tidal surface from the NOAA VDATUM. Thus, Figure 1b shows zones with greater and lesser chances of getting wet (NOAA, 2017a). As shown, there is a high degree of uncertainty in much of the area surrounding the Coral Gables Canal. Inundation maps generated by the Sea-level Rise Viewer do not consider natural processes such as erosion, subsidence, or future construction, and should be used only as a screening-level tool (NOAA, 2017a). Furthermore, these maps only represent sea level rise via a modified bathtub style model. The method accounts for local tidal variability and empirically account for hydro-connectivity but do not explicitly simulate hydrodynamics (NOAA, 2017b). Detailed hydrodynamic modeling with intense quantification of local bathymetry is necessary to develop quantitative estimates of the potential nonlinear relationship between sea-level rise and flooding (Hall et al., 2016). Hydrodynamic models perform a key role in suggesting preventive measures for flood management by identifying flooding risk hotspots and is widely used to study flood inundation in the floodplains (Singh et al., 2020). Neumann and Ahrendt (2013), compared flood simulations performed with a 2-D hydrodynamic model (Mike 21 Flow Model, Danish

Hydraulic Institute) to flooding estimates using a standard bathtub approach. The results showed that for sea-level rise scenarios with the highest water surface elevations, the traditional bathtub method overestimated by 10% the flood area calculated through the MIKE 21 model.

One other source of uncertainty is the tidal elevation data that is used to perform the inundation predictions. NOOA's Sea-level Rise Viewer (2017a) use data from the closest tidal station to the location of interest for mapping flooded areas. However, NOAA tidal stations are oftentimes located kilometers away from specific locations of interest, and tidal elevations may vary (at the location of interest) from the tides observed at NOAA stations. Hydrodynamic modeling could be used for estimating actual tidal elevations occurring at the location of interest, which is essential to robust sea-level rise vulnerability assessment, especially under combined sea-level rise and event-driven water level rise (Anderson et al., 2018).

The combination of gradual sea-level rise with extreme sea-level events that are rare today (tides, surges, etc.) will become more frequent in the future (Oppenheimer et al., 2019; Aucan, 2018; Vitousek et al., 2017). Although the drivers of extreme sea-level events have not significantly changed over the past decades, these events are becoming more severe and frequent (Lang and Mikolajewicz, 2020; Aucan, 2018; NOAA, 2017c). Even small sea-level rise amounts (e.g., 5–10 cm) may more than double the frequency of extreme sea-level events as early as 2030 (Vitousek et al., 2017). Extreme sea-level values occur rarely, but it is those 'high-impact-low-probability' extremes that are required for flood defense, since relative changes in the upper tail of those values may substantially alter the risk for flooding (Lang and Mikolajewicz, 2020; NOAA, 2017c).

The combined effect of mean and extreme sea-level rise could surpass traditional vulnerability estimates based on a simple upward shift in sea level (Lang and Mikolajewicz, 2020). For many coastal locations, the main starting point for coastal planning and decision making should be accounting for future extreme sea-level events through improvement of current observational systems, remote sensing techniques, or hydrodynamic modeling (Oppenheimer et al., 2019; Anderson et al., 2018). There is an urgent need to test plans and policies against extreme water-level events occurring alongside mean sea-level rise (NOAA, 2017c).

In this research, the effect of concurrent mean and extreme sea-level rise on coastal inundation is explored. A three-dimensional hydrodynamic model for Biscayne Bay and the Coral Gables Canal is presented. The model is used to estimate water surface elevations throughout the model domain for scenarios of combined water surface elevation rise. SFRCC (2020) sea-level rise scenarios are combined to observed Irma Hurricane water level rise. Model-generated maps are compared to NOAA's Sea Level Rise Viewer, Climate Central's Surging Seas Risk Zone Map predictions, and Florida Sea-level Scenario Sketch Planning Tool. Conclusions are drawn from the comparison.

2. Methods

2.1 Study area

Biscayne Bay is a coastal water body located in southeast Florida. The area surrounding the Bay, which originally was dedicated to agriculture, has experienced rapid urban growth in the last decades. The combined effects of human activities (urban settlements and agriculture) have increased runoff and nutrient transport from inland watersheds to the Bay. Recent studies have identified increased chlorophyll-a and phosphate concentrations within the bay, which is more evident throughout the northern area and in nearshore areas of central Biscayne Bay, suggesting an urgent need for land use and land cover management to reduce local nutrient wash-off from the watershed to the Bay (Millette et al., 2019; Swart, et al., 2013; Caccia and Boyer, 2007). Santos et al. (2014) established that freshwater discharges into nearshore areas (contaminated by anthropogenic disturbances) have resulted in the fragmentation of the spatial patterning of submerged aquatic vegetation, which is thought to influence the distribution, community composition, and behavior of marine fauna. Man-made canals and waterways carry excess run-off and contaminants, from inland watersheds to Biscayne Bay. One of the main canals, traversing the city of Coral Gables, is the Coral Gables Canal.

The Coral Gables Canal (CGC) is a waterbody 15.70 km long that drains the Tamiami Canal and collects waters from an 18.25 km2 watershed. The Canal run southeast through Coral Gables, draining into Central Biscayne Bay (Figure 2). In rigor, the portion of the Canal that is close to Biscayne Bay is a waterway. For brevity, in this study the whole water body will be identified as Coral Gables Canal. Land use in the watershed is primarily residential and commercial.

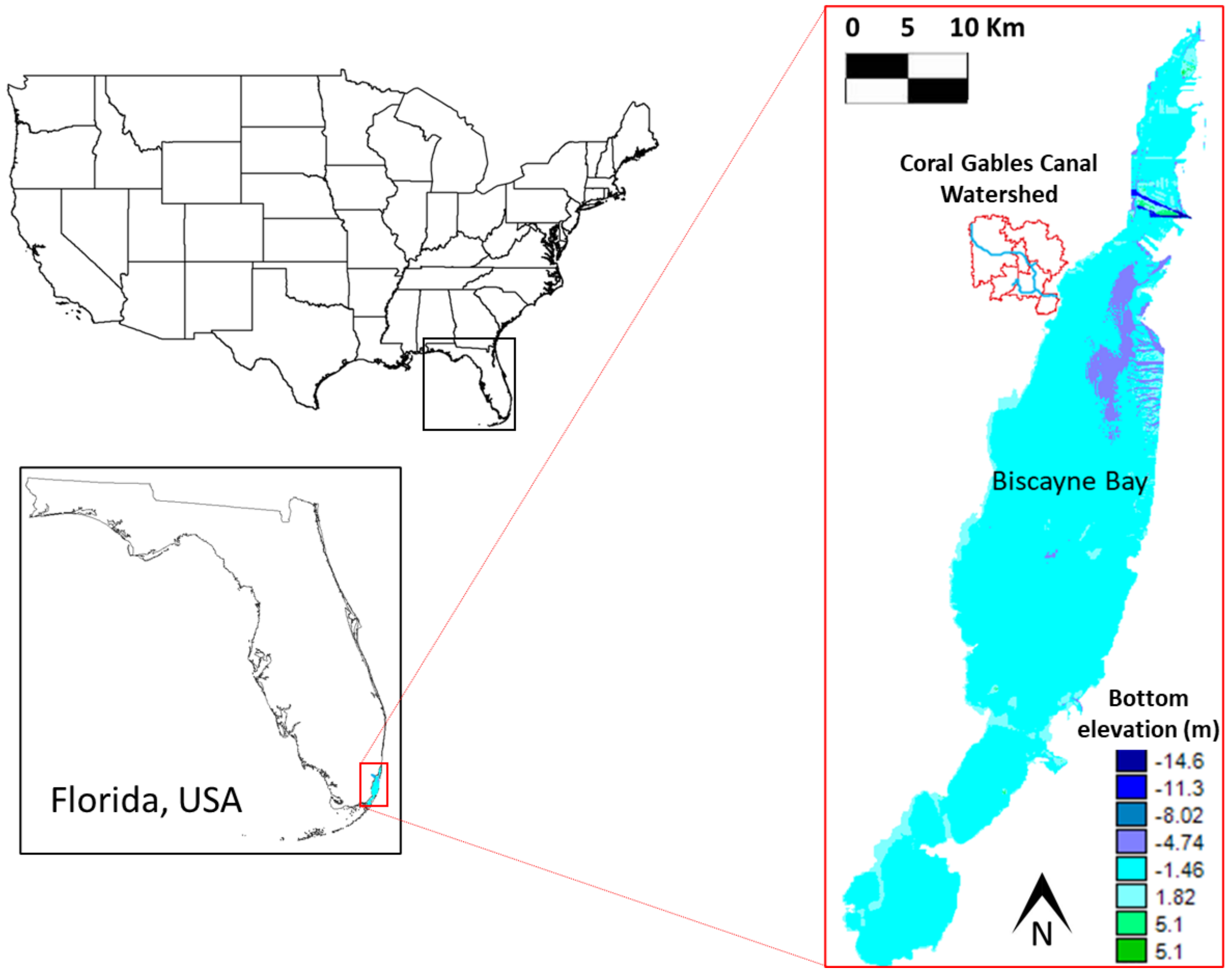

Figure 2. Biscayne Bay and Coral Gables Canal watershed. Bottom elevation in Biscayne Bay (bathymetry) is shown.

Water flow in the canal is interrupted by a control structure (Gate G93), which is located 6.47 km inland (Figure 3). The gate opens intermittently during the rainy season and is closed during the dry season. Water movement in the lower segment of the canal is governed almost entirely by tidal forcing (Bouck, 2017). River stage data is collected at two stations in the CGC: Station G93-H (located immediately upstream from the gate), and Station G93-T located immediately downstream from the gate.

2.2 Basic data

2.2.1 Bathymetry, topography, and bottom roughness

The bathymetry data set used to develop the hydrodynamic model is the 1/3 arc-second Mean Lower Low Water bathymetric DEM produced by NOAA's National Ocean Service (NOAA/NOS, 2020). This data set is based on a hydrographic survey data for Biscayne Bay. The bathymetric data (provided as a NETCDF data cube, NAVD) was geo-processed and projected to UTM (Zone 17 North, WGS84) coordinates. The resulting data raster (horizontal spatial resolution 9.27 m x 9.27 m, vertical accuracy 0.01 m) is shown in Figure 2. This dataset was used for generating the computational grid of Biscayne Bay.

The topographical data used to characterize the topography of the watershed and the bathymetry of the Coral Gables Canal was a 5 m cell size Digital Elevation Model (DEM). The elevation units, expressed in centimeters, have NAVD88 as reference datum. The dataset is provided in Albers Equal Area Conic HARN projection by the University of Florida GeoPlan Center (2020).

2.2.2 Tidal, river stage, river flow, and wind data

Hourly data for water surface elevation (WSE), air temperature, wind speed, and wind direction at Virginia Key Station (Figure 3) were obtained from NOAA (2020) and used for setting up ocean boundary conditions. River stage data for main streams draining to Biscayne Bay (canals, creeks, etc.) were obtained from the South Florida Water Management District's DBHYDRO platform (SFWMD, 2020), and used to calibrate and validate the hydrodynamic model. Stream flows from main tributaries to the Bay (freshwater inputs shown in Figure 3) were also obtained from SFWMD

(2020). All data were transformed to the metric system, NAVD vertical reference, and GMT zone. Wind and temperature data at Virginia Key Station were collected at 8.5 m above mean sea-level.

2.3 Hydrodynamic modeling

In this research, the Environmental Fluid Dynamic Code (EFDC) was used as the modeling tool. EFDC (Hamrick, 1992) is a 3-D model that is used extensively in the United States (Alarcon et al., 2014) and abroad. It is currently used by federal, state, and local agencies, consultants, and universities. The EFDC version used was the Dynamics Solutions LLC's EFDC_DSI Version 2020. Throughout this paper, the EFDC_DSI version will be denominated EFDC for brevity. EFDC solves the three-dimensional, primitive-variable, vertically-hydrostatic, free-surface, turbulent averaged equations of motions for a variable-density fluid. The model uses Cartesian or curvilinear-orthogonal horizontal coordinates. Dynamically coupled transport equations for turbulent kinetic energy, turbulence length scale, salinity, and temperature are solved (Alarcon et al., 2014). The model is forced by boundary loadings (water velocity, water surface elevation, stream flow inputs), and atmospheric conditions (e.g., temperature, pressure, wind shear, precipitation). The equations are solved by EFDC through the implementation of a semi-implicit, conservative finite-volume finite-difference algorithm with either 2 or 3-level time-stepping. The semi-implicit scheme is based on external mode splitting with the external mode being implicit with respect to the water surface elevation and the internal mode being implicit with respect to vertical turbulent momentum diffusion (Tetratech, 2002).

2.3.1 Computational grid

Generating an efficient computational representation of the study area required iterating with the following variables: computational grid spatial resolution, location of boundary conditions, curvilinear versus cartesian coordinates, and numerical criteria (time-step, numerical algorithm, etc.). The resulting computational representation of Biscayne Bay and the Coral Gables Canal is shown in Figure 3.

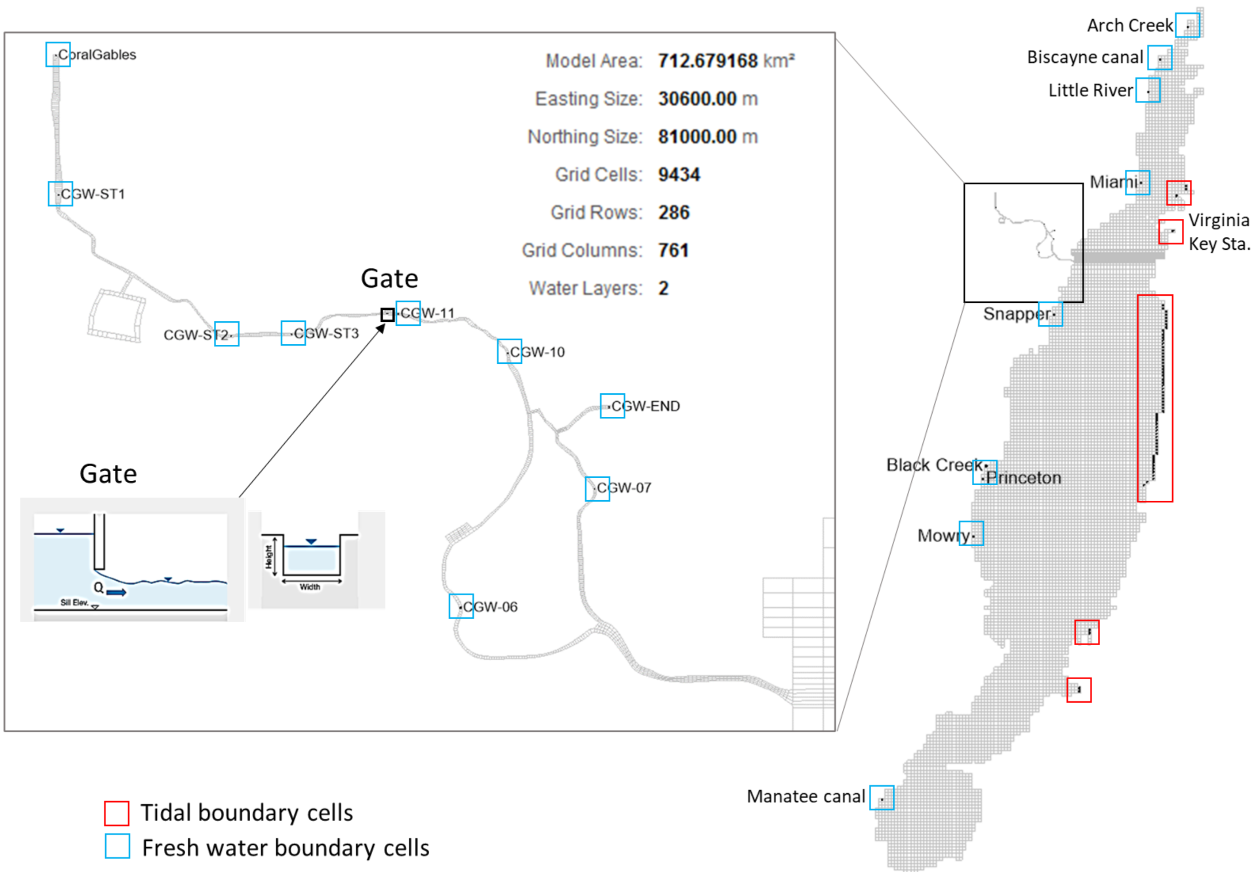

Figure 3. Computational grid for the study area. Open ocean boundary cells and freshwater boundary cells are shown. A cartesian grid representing Biscayne Bay connects to a curvilinear grid representing the Coral Gables Canal.

The computational mesh shown in Figure 3 consists of over 9,400 grid cells. The Bay is represented in cartesian coordinates and the Canal consists of curvilinear cells. To have an efficient transfer of information between the Bay portion and the Canal portion, cell sizes near the outfall of the canal to the Bay were gradually decreased until reaching similar order of magnitude in size as the cells of the canal. The computational mesh includes a representation of gate G93 (located on the Coral Gables Canal), which operation is simulated according to the rules of operation reported for the hydraulic structure by DBHYDRO.

Boundary cells are also shown in Figure 3. Tidal boundary cells are located at the eastern borders of the grid and provide seawater inputs to the system using data from Virginia Key Station (tidal and wind). Fresh water boundary cells shown corresponding to Arch Creek, Biscayne canal, Little River, Miami River, Snapper Creek, Black Creek, Princeton canal, Mowry canal, and Manatee canal are shown.

2.3.2 Goodness of fit of simulated data

Statistical indicators of fit between forecasted and observed data and corresponding statistical errors were computed to quantify the quality of simulated data. The following indicators were used for assessing statistical fit: coefficient of determination (R^2), Nash–Sutcliffe coefficient (NSE). The root-mean-squared-error to standard deviation ratio (RSR) was calculated to quantify statistical errors. The Kling-Gupta efficiency index (K-G) was used to measure goodness of fit as well as bias of simulated data from observed data. Table 1 summarizes all the statistical indicators used and their corresponding ranges of acceptability.

Table 1. Statistical indicators of goodness of fit.

Indicators of Fit	Formulae	Range
Root-mean-squared-error to standard deviation ratio, $RSR = \frac{RMSE}{STDEV_{Obs}}$	$\frac{\sqrt{\sum_{i=1}^{n}(Y_i^{Obs} - Y_i^{Sim}).^2}}{\sqrt{\sum_{i=1}^{n}(Y_i^{Obs} - Y_i^{Mean}).^2}}$	RSR < 0.7 (*)
Coefficient of determination, R^2	$\left(\sqrt{\frac{\sum_{i=1}^{n}(Y_i^{Sim} - Y_i^{Mean}).^2}{\sum_{i=1}^{n}(Y_i^{Obs} - Y_i^{Mean}).^2}}\right)^2$	$R^2 > 0.5$ (*)
Nash-Sutcliffe efficiency, *NSE*	$1 - \frac{\sum_{i=1}^{n}(Y_i^{Obs} - Y_i^{Sim}).^2}{\sum_{i=1}^{n}(Y_i^{Obs} - Y_i^{Mean}).^2}$	NSE > 0.5 (*) (**) NSE > 0.3 (***)
Kling-Gupta efficiency, *K-G*	$1 - \sqrt{\left(\frac{Y_{Sim}^{Mean}}{Y_{Obs}^{Mean}} - 1\right)^2 + \left(\frac{STDEV_{Sim}}{STDEV_{Obs}} - 1\right)^2 + (R-1)^2}$	K-G > 0.5 (**)
Y_i^{Obs} = Observed SST concentration Y_i^{Sim} = Simulated SST concentration Y_{Obs}^{Mean} = Mean of observed SST concentration Y_{Sim}^{Mean} = Mean of simulated SST concentration, n = Total number of daily SST concentrations		(*) Moriasi et al., 2007. (**) Knoben et al., 2019. (***) Allen et al., 2007.

The range for the Kling-Gupta indicator (K-G) shown in Table 1 is suggested by Knoben et al. (2019). The ranges for RSR, R^2, and NSE proposed by Moriasi et al. (2007) correspond to monthly time-step simulations. Generally, as the evaluation time-step decreases, less strict performance rating is warranted. Since the simulations in this research are generated at hourly time-step, the

Moriasi et al. (2007) ratings shown in Table 1 could be allowed 20% flexibility as proposed by the cited authors.

2.4 Sea-level rise scenarios

The unified sea-level rise projection for Southeast Florida (SFRCCC, 2020) presents sea-level rise projections using a reference year of 2000 and historical tidal elevations recorded at NOAA's Key West Tidal station. The document recommends interpolating the projection values depending on the year for which the relative sea-level rise is desired. Figure 4 shows interpolated sea-level rise projections for years 2050, 2100, and 2120, for three sea-level rise scenarios: Intergovernmental Panel on Climate Change (IPCC) projection, NOAA Intermediate-High projection, and NOAA High projection. Since the projections are based on year 2000, those sea-level rise values were adjusted in this research so that the relative sea-level rise that occurred until the year of interest is accounted for (Figure 4). Table 2 summarizes the interpolation of sea-level rise for year 2017.

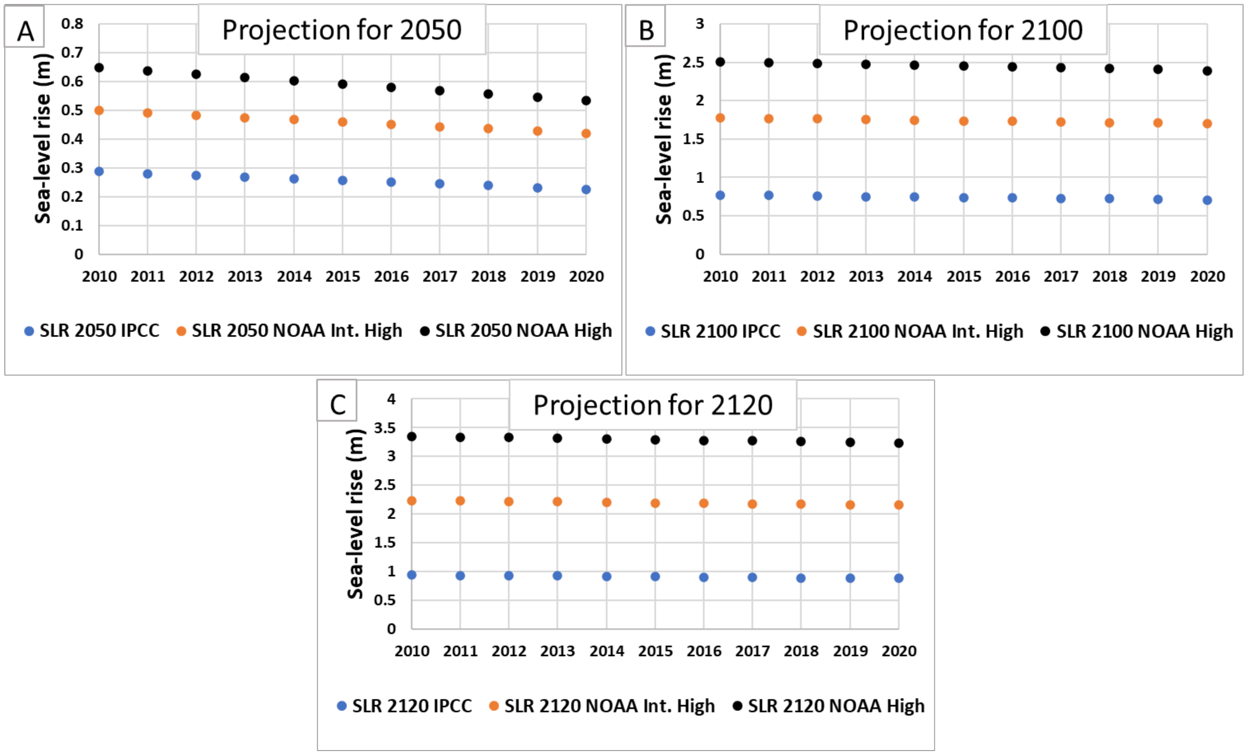

Figure 4. Interpolated sea-level rise projections for years 2050, 2100, and 2120. Scenarios: A) Intergovernmental Panel on Climate Change (IPCC) projection, B) NOAA Intermediate-High projection, and C) NOAA High projection.

Table 2. Sea-level rise for year 2017 for scenarios NOAA Intermediate High, and NOAA High.

Year	NOAA Int. High	NOAA High
2060	0.63	0.85
2100	1.72	2.43
2120	2.18	3.27

The NOAA Intermediate High regional projection (Sweet et al., 2017) is recommended for infrastructure projects requiring an essential factor of safety related to inundation: evacuation routes planned for reconstruction, communications/energy infrastructure, critical government, and financial facilities/infrastructure (SFRCCC, 2020). The NOAA High projection should be used for assessing high-risk of inundation for existing and planned critical infrastructure: nuclear power plants, wastewater treatment facilities, levees or impoundments, bridges along major evacuation routes, airports, seaports, railroads, and major highways (SFRCCC, 2020). In this research, the scenarios included for inundation/flooding simulations are the NOAA Intermediate High and the NOAA High projections.

2.5 Baseline for comparison of sea-level rise scenarios

Since the sea-level rise projected values decrease depending on how current the reference year, an analysis of historical tidal elevations was performed to identify which year would be the baseline for comparison in this study. Figure 5 shows daily maximum water surface elevations observed at Virginia Key, and G93-T stations (the latter is located in the Coral Gables Canal) from 01-01-2012 to 12-31-2018. As shown, the maximum observed tidal elevation at the Virginia Key station was 1.17 m (on September 10, 2017), corresponding to a tidal elevation of 1.73 m at the G93-T station. The event that produced such high readings was Hurricane Irma.

Figure 5 also depicts the difference between observed water surface elevation at both stations (WSE at G93-T minus WSE at Virginia Key). The cumulative WSE curve shows that observed WSE at G93-T are mostly greater in value than those corresponding to Virginia Key station. As shown, the slope of the cumulative WSE difference curve is mostly positive especially after year

2016, meaning that observed WSE at G93 become increasingly greater than those at Virginia Key after that year. The greatest difference occurs during the Irma event (0.56 m). Although during the Irma Hurricane flooding was not reported in Coral Gables, the impact of the occurrence of such an event under future sea-level rise scenarios is worth exploring.

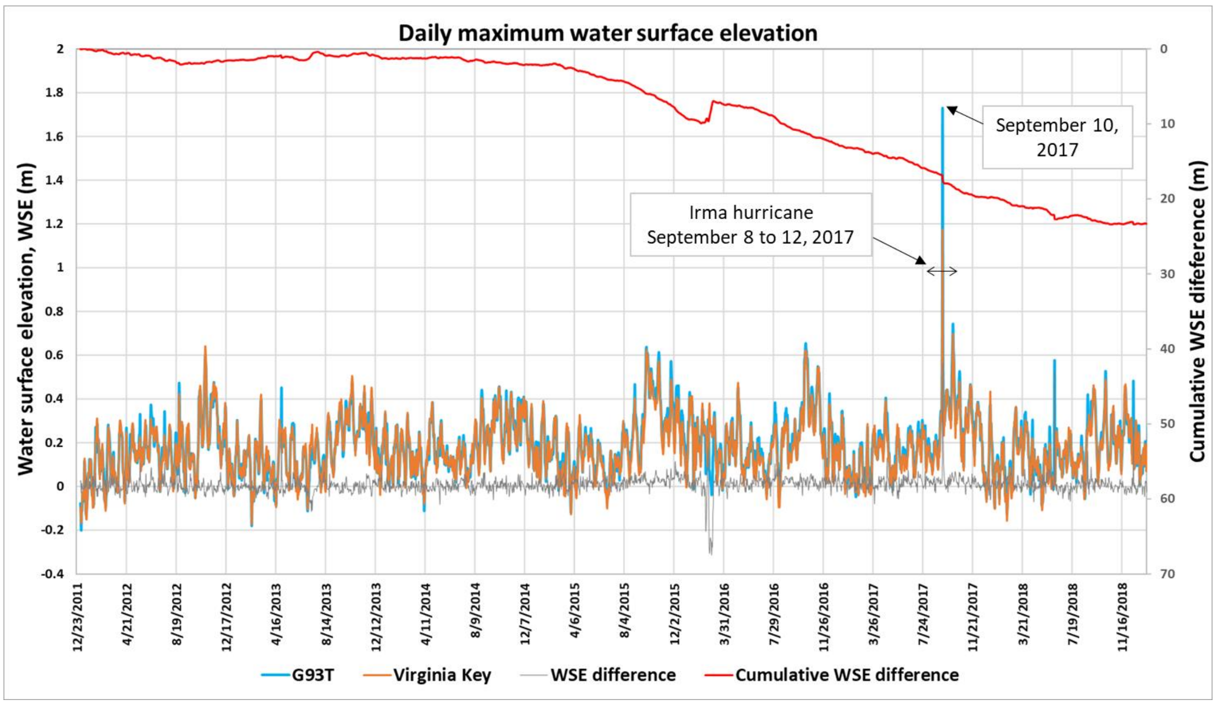

Figure 5. Daily maximum water surface elevations. WSE difference and Cumulative WSE difference are computed according to WSE at G93-T minus WSE at Virginia Key.

The exploration of daily maximum water surface elevations allowed the identification of the Irma Hurricane as a representative extreme event if it were to occur under risen sea-level conditions. Next, the effects of gate G93 on the hydrodynamic regime of the canal under extreme high-water conditions should be ascertained. Figure 6 shows a comparison of observed hourly water surface elevations at stations: Virginia Key, G93-T (station located downstream to the gate), and G93-H (station located upstream to the gate). Figure 6 shows that hydrodynamic processes (momentum, wind, waves) cause the water surface elevation at gate G93-T and G93-H to be slightly higher than those observed at Virginia Key, under normal conditions. However, during the Irma event, water surface elevations in the canal were observed to be noticeably higher (50% to 400%). Data collected at both canal stations (G93-H and G93-T) show a similar trend. Therefore, such an event would affect the entire canal, upstream and downstream of the gate, similarly.

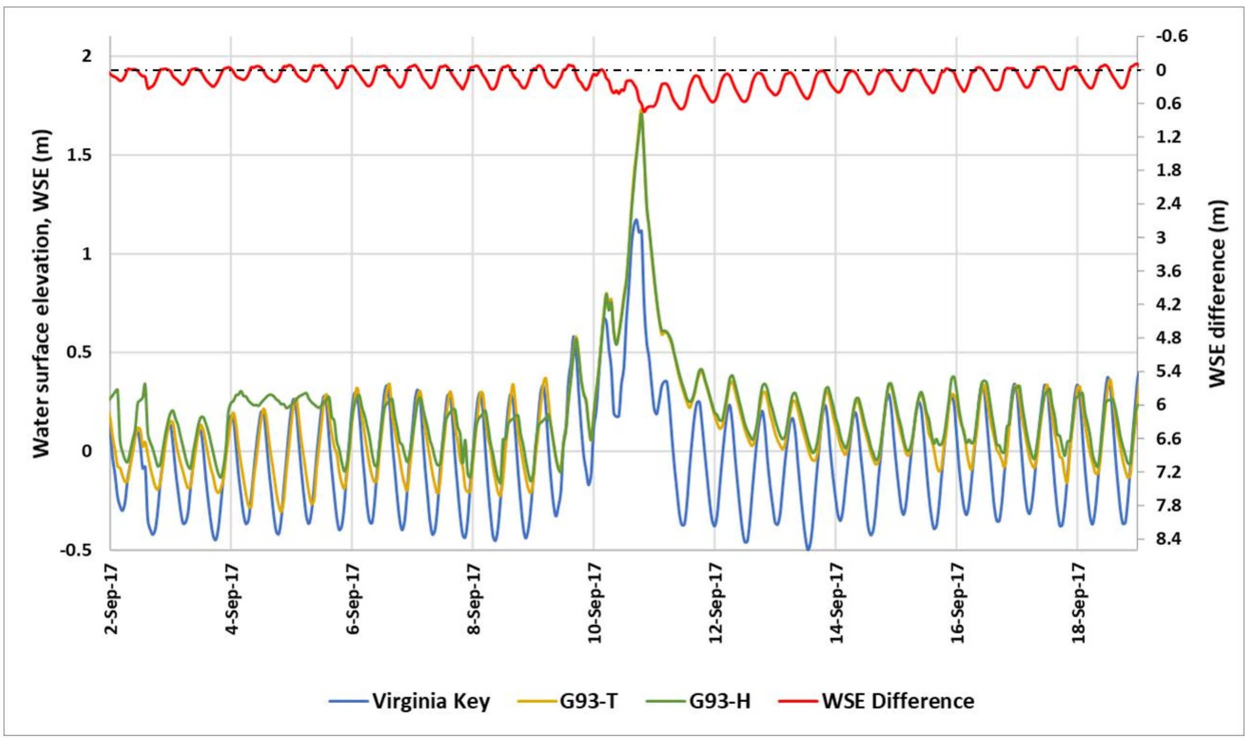

Figure 6. Comparison of water surface elevations at stations Virginia Key Station, G93-H, and G93-T. The secondary vertical axis at the right shows the WSE difference between WSE at G93-T and WSE at Virginia Key. Station G93-H registered practically the same WSE during Irma Hurricane.

Figure 6 also illustrates the magnitude of the difference in water surface elevations between Virginia Key and G93 stations. The station upstream to the gate (G93-H) recorded practically the same WSE data as station G93-T (located downstream to the gate), meaning that the gate was open during the Irma event. Figure 6 shows the WSE difference: G93-T WSE minus Virginia Key WSE. Peak water surface elevations were the greatest during the extreme Irma event. It would be expected that under sea-level rise conditions, the WSE difference observed during the Irma event would be similar. Figure 6 reinforces the importance of exploring the consequences of an Irma-like hurricane occurring under projected sea-level rise scenarios.

2.6 Flooding area determination

The sea-level rise values corresponding to years 2060, 2100, and 2120 (shown in Table 2) were each added to the water surface elevations observed during Irma Hurricane, and specified as ocean boundary conditions of the validated hydrodynamic model. Therefore, six sea-level rise scenarios were modeled: three corresponding to NOAA Intermediate High, and three corresponding to NOAA High. The hydrodynamic model was used to calculate hourly water surface elevations for Biscayne Bay and the Coral gables Canal for those scenarios.

The flooding areas were determined using the water surface elevations (WSE) calculated by the hydrodynamic model of the Coral Gables Canal, and the identification of hydrologically connected cells in its watershed DEM. As described in previous sections, the topography of the area was characterized by a 5-meter DEM in which elevations are in centimeters (NAVD). The elevation in each cell of the DEM was compared to the WSE predicted by the hydrodynamic model. All cells with topographic values lower than the predicted WSE were considered flooded. Hydrological connectivity (passage of water from one cell to another) was considered by requiring that (in addition to being below the flood level) the cells must be hydrologically connected. Several studies have applied a similar procedure to map coastal and inland inundation around the globe (Yunus et al., 2016). NOAA follows a similar approach for mapping sea-level rise inundation (NOAA, 2017a).

3. Results

3.1 Hydrodynamic calibration

Calibration of the hydrodynamic model was performed comparing predicted hourly water surface elevations (WSE) to observed data at four locations inside Biscayne Bay and the Coral Gables Canal. Figure 7 shows stations MRMS4, G93T, S123T, S20GT, which data were used for calibration and validation of the hydrodynamic model.

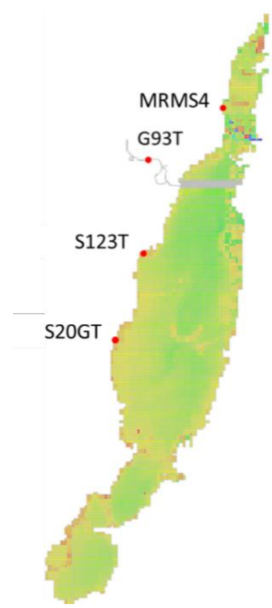

Figure 7. Stations collecting water surface elevation data at Biscayne Bay. Data from MRMS4, G93T, S123T, S20GT stations were used for calibration and validation of the hydrodynamic model.

Figure 8 shows the results of the comparison for year 2014. The locations correspond to stations that collect water surface elevation or river stage data.

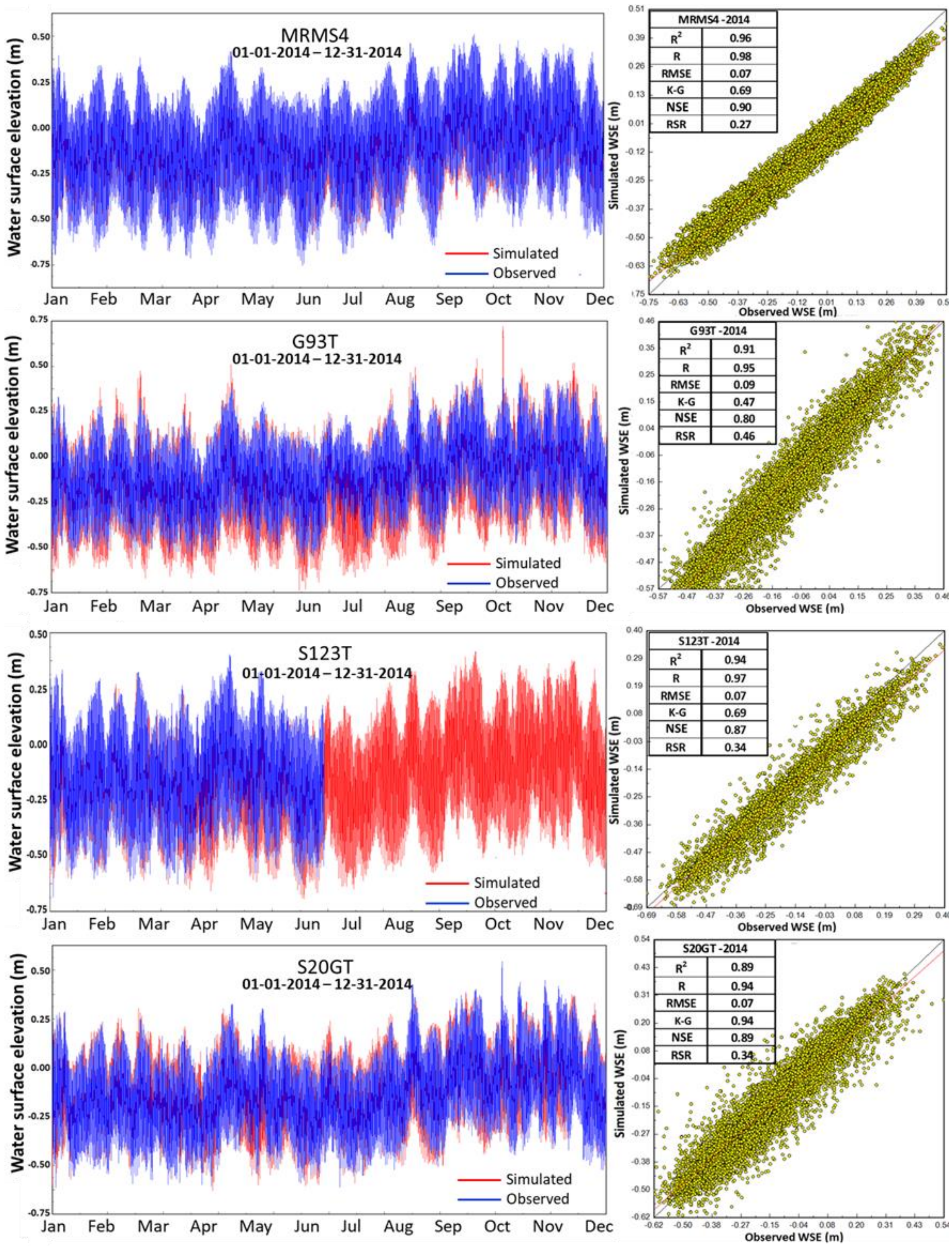

Figure 8. Hydrodynamic calibration for year 2014. Observed and simulated WSE time-series and corresponding scatterplots for four locations in Biscayne Bay are shown.

Model calibration was conducted for 2014 (Figure 8) and 2015 (Figure 9). As shown in Figure 8, the comparison of simulated versus observed WSE data results for year 2014 produced good statistical indicators of fit: $R^2 > 0.89$, NSE > 0.80, K-G > 0.47, RMSE< 0.09, RSR < 0.43. Overall, the statistical indicators show good agreement between simulated and observed water surface elevations. In particular, RMSE values were low (<0.09). For subsequent comparisons, the RMSE not calculated because the ratio of RMSE to standard deviation of the observed data (RSR) encompasses the error captured by RMSE.

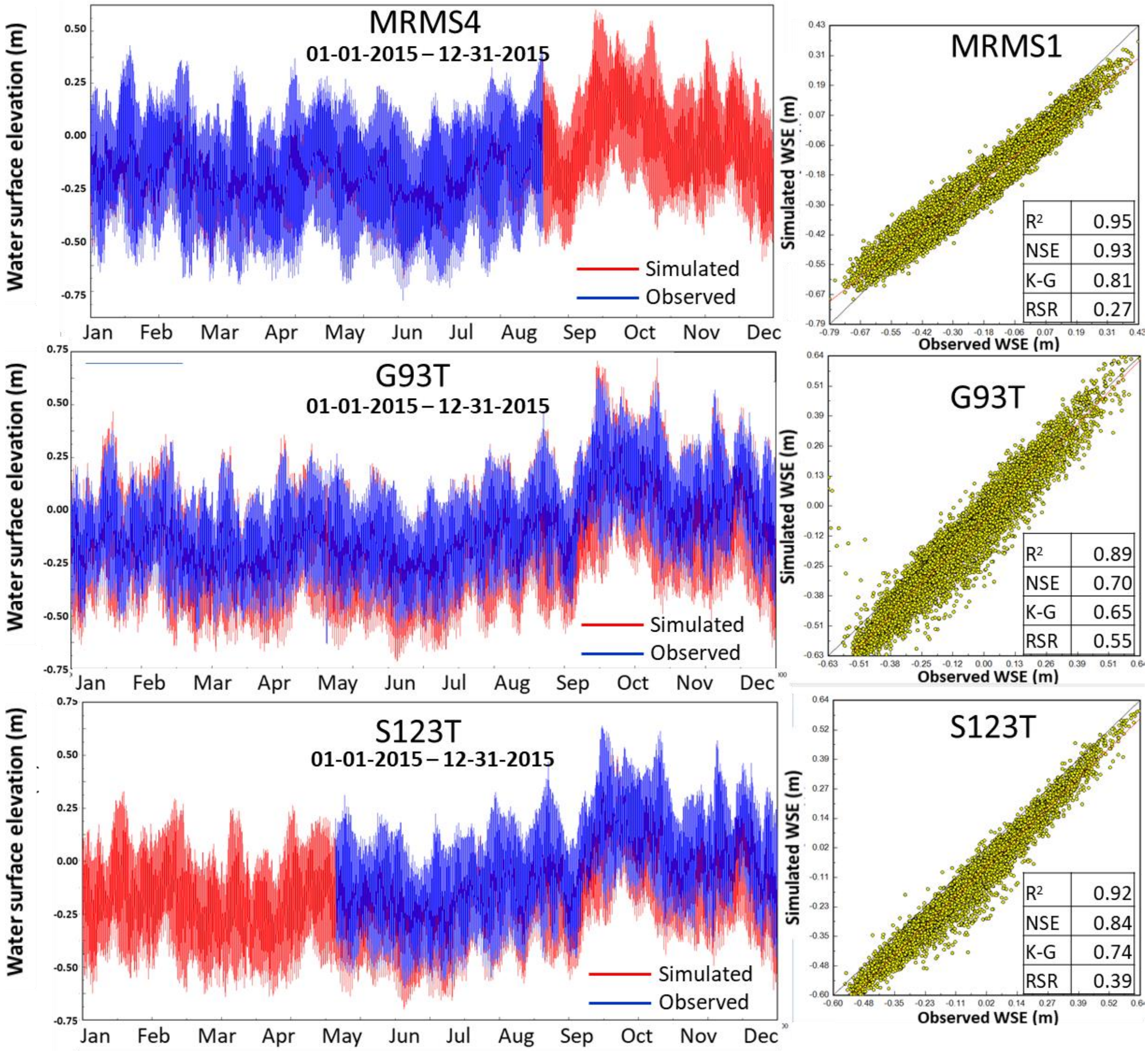

Figure 9. Hydrodynamic calibration for year 2015. Observed and simulated WSE time-series and corresponding scatterplots for four locations in Biscayne Bay are shown.

As shown in Figure 9, the statistical indicators for year 2015 are also good: $R^2 > 0.89$, NSE > 0.70, K-G > 0.65, and RSR < 0.55. Station S20GT is not included in the 2015 calibration because observed data for 2015 at this station was sparse. The overall quality of the goodness of fit indicators is good, therefore the hydrodynamic model could be considered calibrated.

3.2 Hydrodynamic validation

Hydrodynamic validation was performed for year 2017, following the analysis on tidal elevations for that year (Section 2.4). Figure 10 shows statistical indicators for validation. The goodness of fit between simulated and observed data for northern Biscayne Bay is described by the following statistics: $R^2 > 0.69$, NSE > 0.64, K-G > 0.55, and RSR < 0.60. The model has some limitations on replicating observed data at S20GT station ($R^2 = 0.48$, NSE = 0.33, K-G = 0.63, and RSR = 0.82). However, NSE and K-G statistics are within the ranges of acceptability presented in Table 1, and R^2 and RSR are within the 20% flexibility attributed to those statistics as suggested by Moriasi et al. (2007). Therefore, the hydrodynamic model is validated.

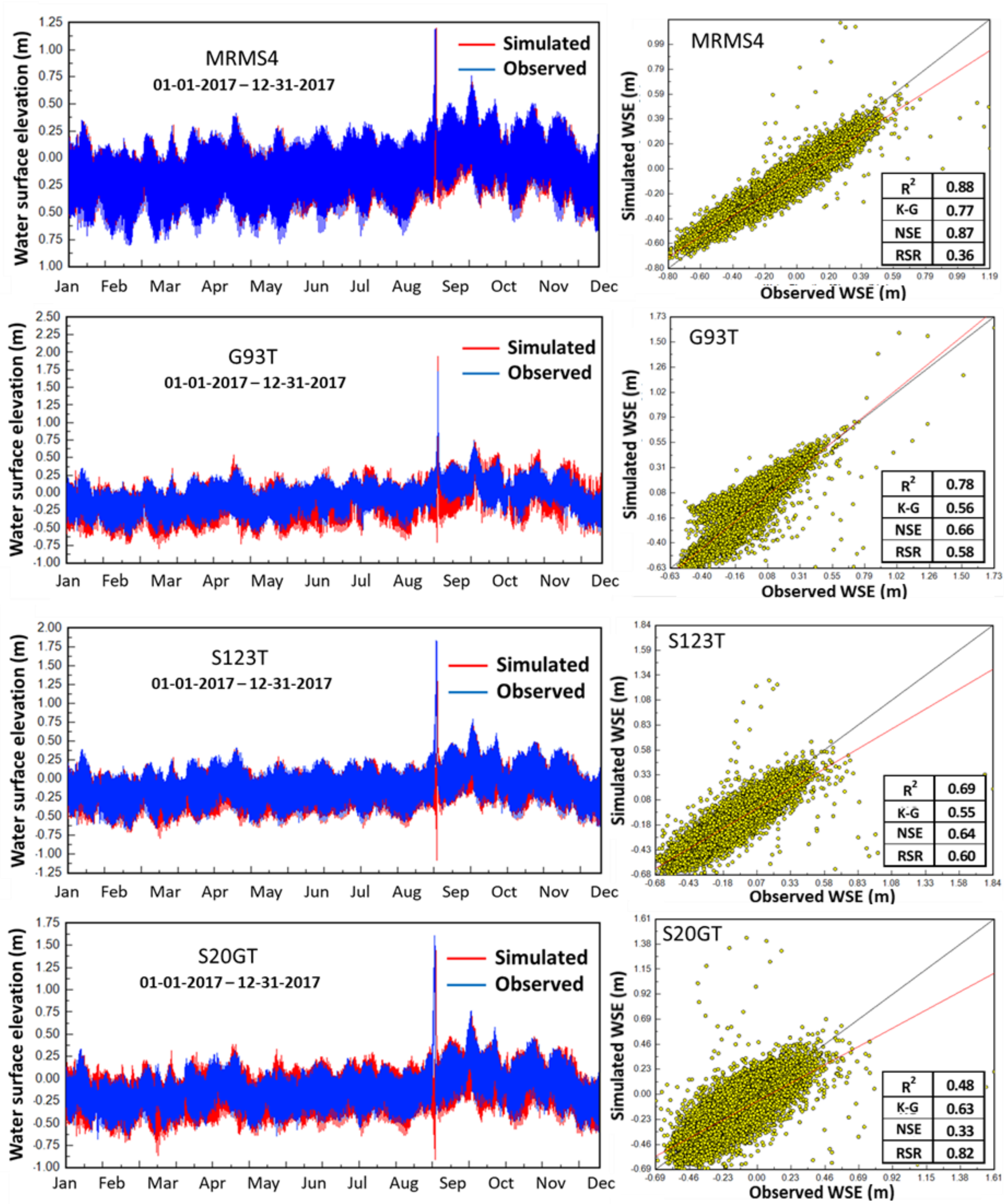

Figure 10. Hydrodynamic validation.

3.3 Comparison of model-simulated flood areas for year 2100 to online SLR simulators

The calibrated and validated model was used to predict water surface elevations in the CGC for year 2100 so that the model results could be compared to the following online sea-level rise tools Surging seas Climate central (Climate Central, 2021), NOAA Sea-Level Rise Viewer (NOAA, 2121), and Florida Sea-level Scenario Sketch Planning Tool (University of Florida, 2021). To simulate scenarios NOAA Intermediate High, and NOAA High, the following sea-level rise values were added to the ocean boundary conditions: 1.73 m, and 2.43 m, respectively (from Table 2). The simulation period captures an event equivalent to the Irma hurricane. Figure 11 shows water surface elevations for several locations in the Coral Gables Canal. As shown, water surface elevations along the canal are very similar with an average maximum value of 3.67 m. This value is greater by 16% than the NOAA Extreme scenario projection of 3.16 m sea-level rise, and greater by 44% than the NOAA High scenario (2.55 m). This is because Sea Leve Rise viewer use data from Virginia Key station and does not account for local tidal variability.

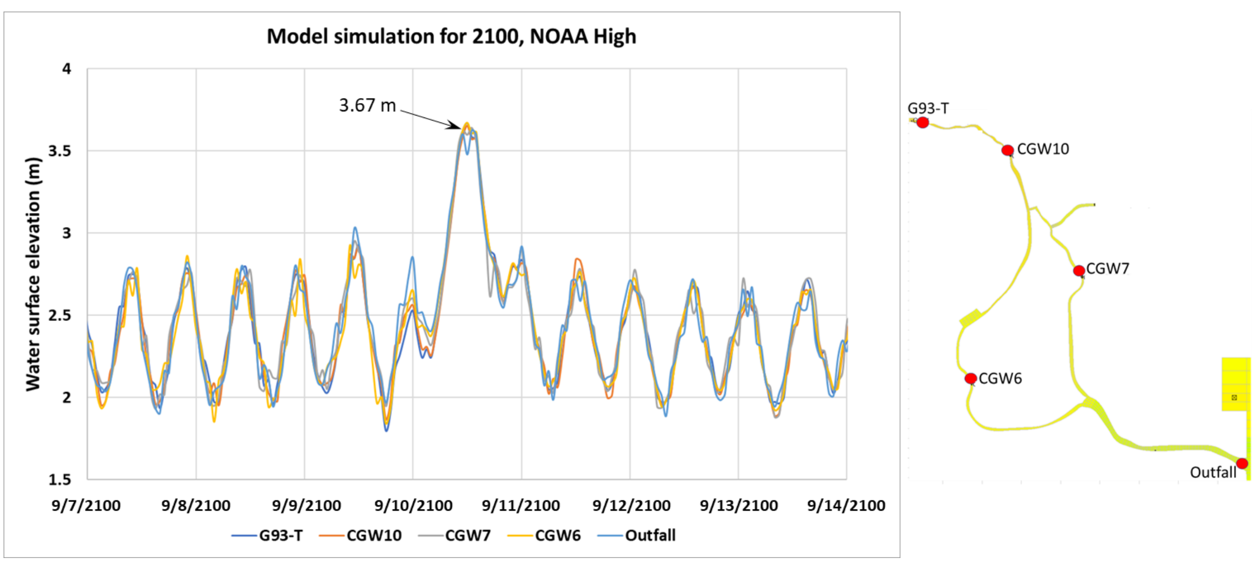

Figure 11. Model-simulated water surface elevations in the Coral Gables Canal.

The impact of the estimations of concurrent sea-level rise on inundation mapping is substantial. Figure 12 shows a comparison of flooding areas obtained in this research to estimations made by the online tools. The online simulators were set up to predict year-2100 inundation under NOAA High scenario (2.55-meter water level). The tools generate very similar maps (Figure 12); however, the inundation coverage is smaller than the inundated area estimated in this research: Climate Central predicts 22% smaller inundated area, NOAA Sea-Level Rise Viewer and Florida Sea-level Scenario Sketch Planning Tool simulates 29% smaller inundation area. This result was expected since the maximum tidal elevation predicted by the hydrodynamic model is greater than the NOAA High predicted water level. Nevertheless, the results confirm that the combined effect of mean and extreme sea-level rise surpass traditional estimates based on a simple shift of the sea level distribution. Also, the results clearly show that a robust sea-level rise vulnerability assessment should be based on local estimations of extreme tides. Local estimations of water surface elevations under combined extreme-event and mean sea level rise should be the starting point for coastal planning and decision making.

Besides providing a more realistic inundation map, this research also provides detailed spatial distributions and magnitudes of water depths. This could be significant for flooding/inundation risk management decisions. Having an accurate spatial estimation of inundation coverage and water depths could contribute to better assessing high-risk of inundation for existing and planned critical infrastructure (SFRCCC, 2020).

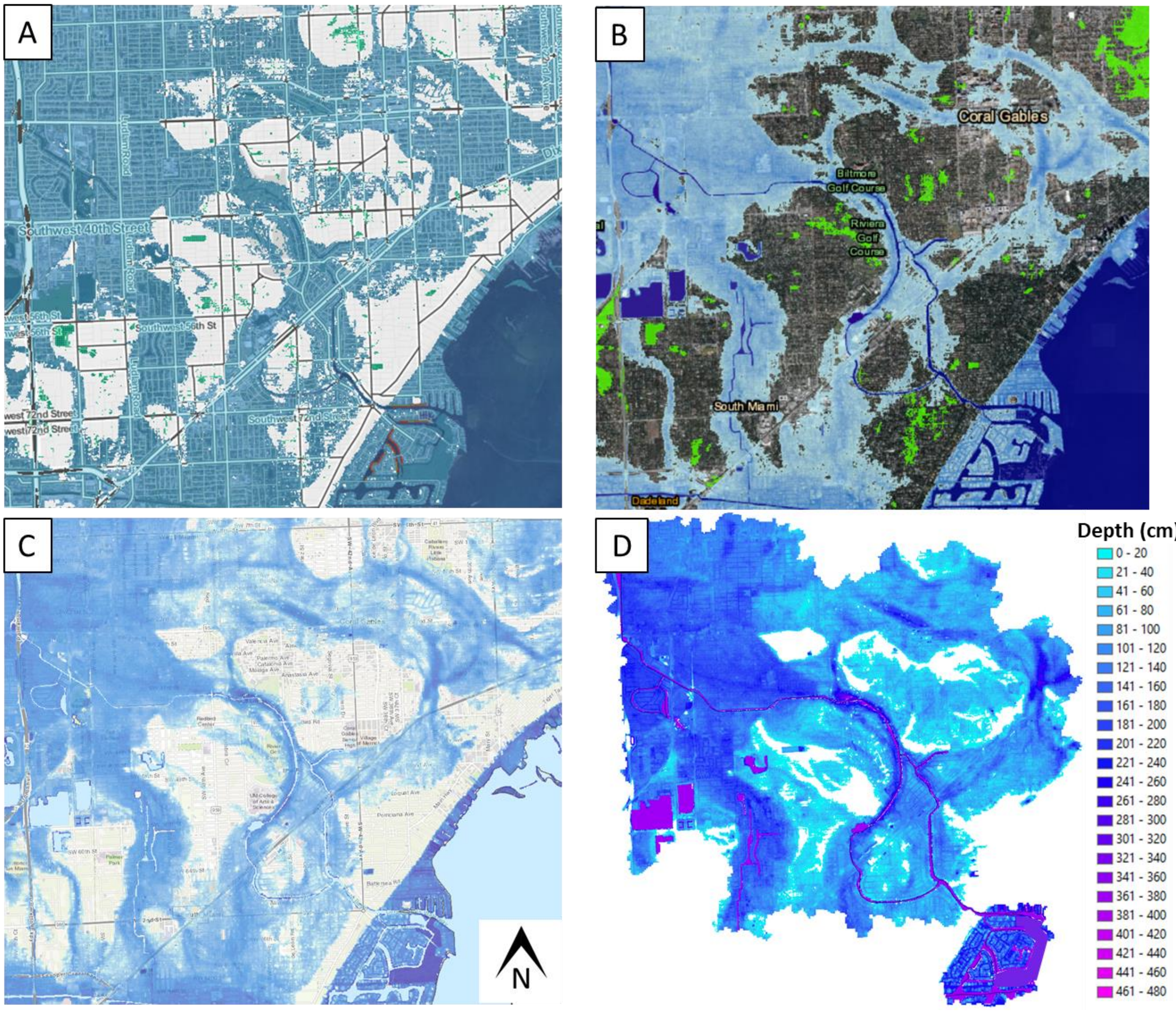

Figure 12. Comparison of inundation maps for year 2100, NOAA High scenario. A) Surging seas Climate central, B) NOAA Sea-Level Rise Viewer, C) Florida Sea-level Scenario Sketch Planning Tool, D) map produced in this research.

A similar comparison was performed for the NOAA Intermediate High scenario for year 2100. Under this scenario, the hydrodynamic model predicts that water surface elevations in the Coral Gables Canal and surrounding areas (during an event similar to hurricane Irma) would reach an average value of 2.96 m (Figure 13). The water surface elevation estimation for the NOAA

Intermediate High scenario provided by the Sea-level Rise Viewer (NOAA, 2021) is 1.83 m (62% smaller than the value calculated in this research). This difference between peak water elevations produced an underestimation of inundated areas by the online tools, compared to the flooded areas estimated in this research (Figure 14).

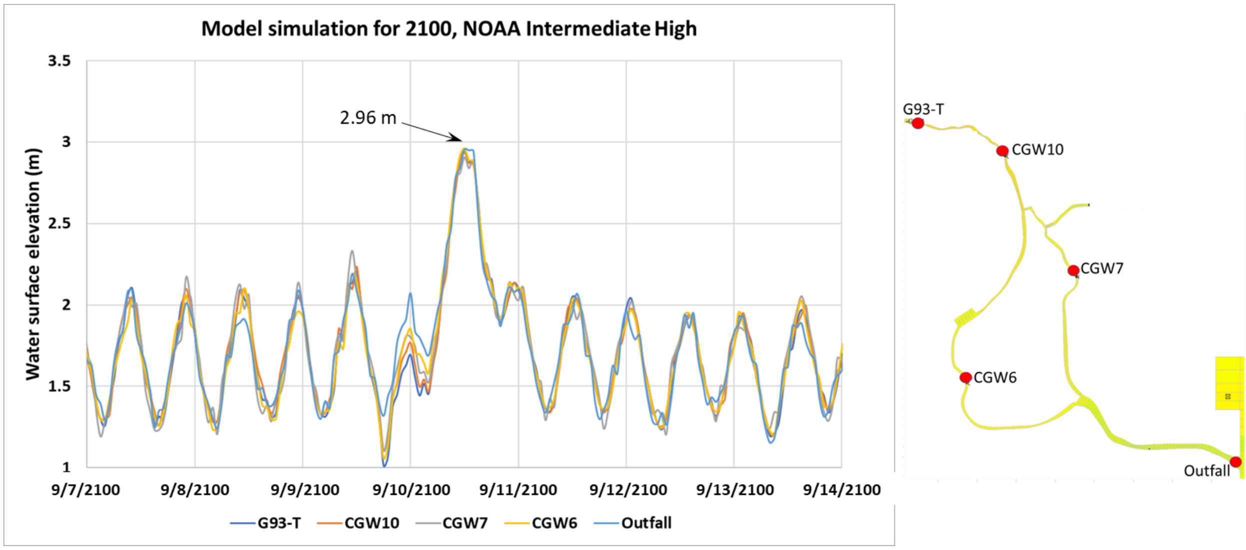

Figure 13. Model-simulated water surface elevations in the Coral Gables Canal.

Figure 14 shows the results provided by the online tools for NOAA Intermediate High scenario. As shown, the inundation area estimated by those tools is smaller than the inundation area calculated in this research. While the model calculates that the inundated area covers 27 km^2, Surging Seas Climate Central and NOAA Sea-Level Rise viewers estimate that around only 7.5 km^2 will be inundated (72% smaller). The Florida Sea-level Scenario Sketch Planning tool estimates that approximately 4 km^2 will be flooded (85% smaller). Again, the advantage of calculating more realistic WSE at the local scale, allowed for a more detailed estimation of inundated areas and water depths.

As stated in Sweet et al. (2017) and SFRCCC (2020), the NOAA Intermediate High scenario is recommended for infrastructure projects requiring an essential factor of safety related to inundation (evacuation routes, communications and energy infrastructure, government and financial facilities and infrastructure). Since the combination of gradual sea-level rise with extreme sea-level events will become more frequent in the future (Oppenheimer et al., 2019; Aucan, 2018; Vitousek et al., 2017), performing a realistic estimation of the combined consequences is paramount for planning flood defense. In this context, the inundation maps generated in this research would help toward the management measures required for providing a safety factor to potential critical projects to be undertaken in the area.

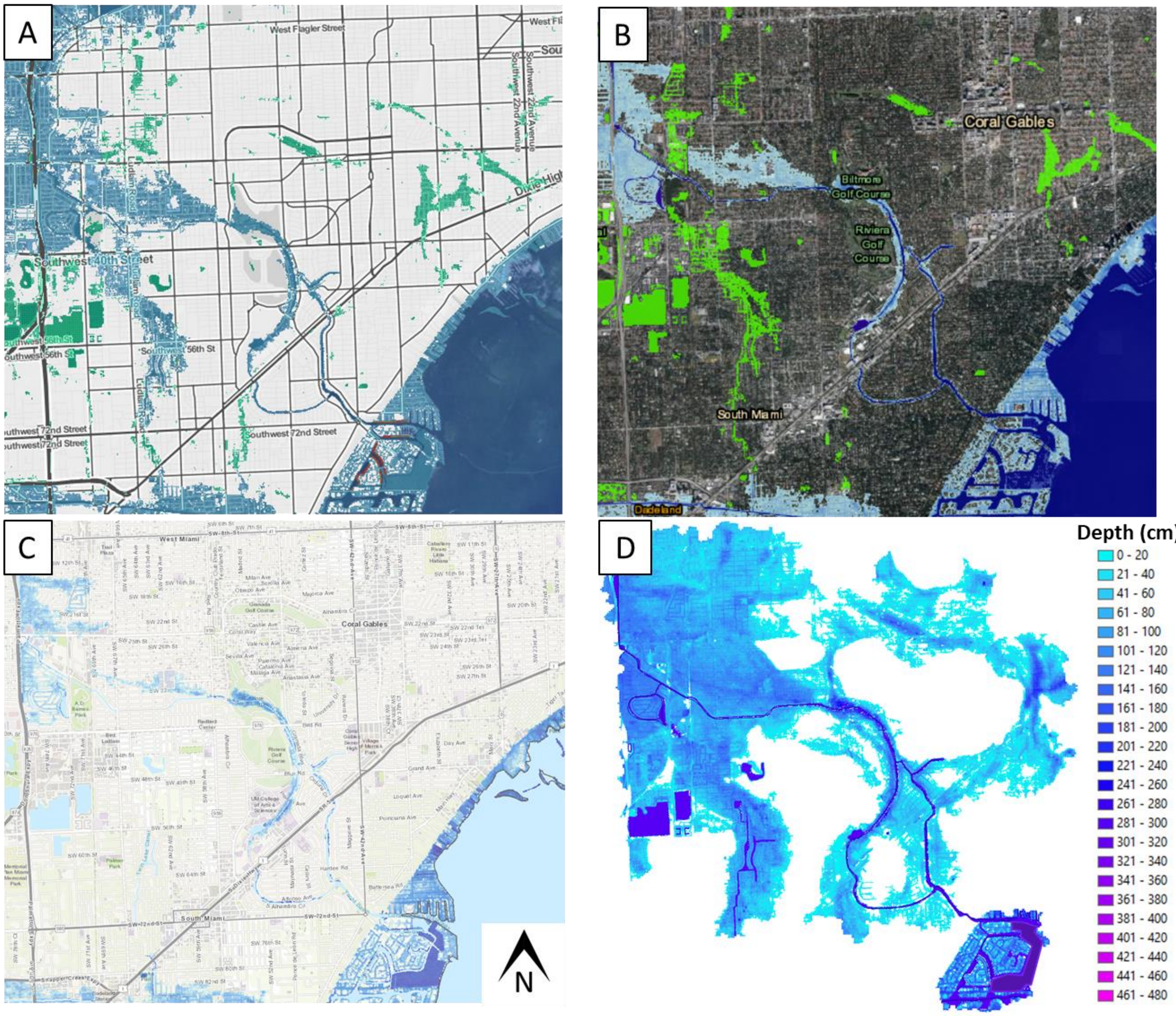

Figure 14. Comparison of inundation maps for year 2100, NOAA Intermediate High scenario. A) Surging seas Climate central, B) NOAA Sea-Level Rise Viewer, C) Florida Sea-level Scenario Sketch Planning Tool, D) map produced in this research.

3.4 Comparison of inundation areas for 2060, 2100, and 2120, to a 2017 inundation map

Summarized results for years 2017, 2060, 2100, and 2120 are presented in Figures 15 and 16. Simulations corresponding scenarios NOAA Intermediate High, and NOAA High were generated.

Figures 15 and 16 show the limits of the Coral Gables Canal watershed and sub-watersheds and could be used for establishing risk management measures per sub-watershed.

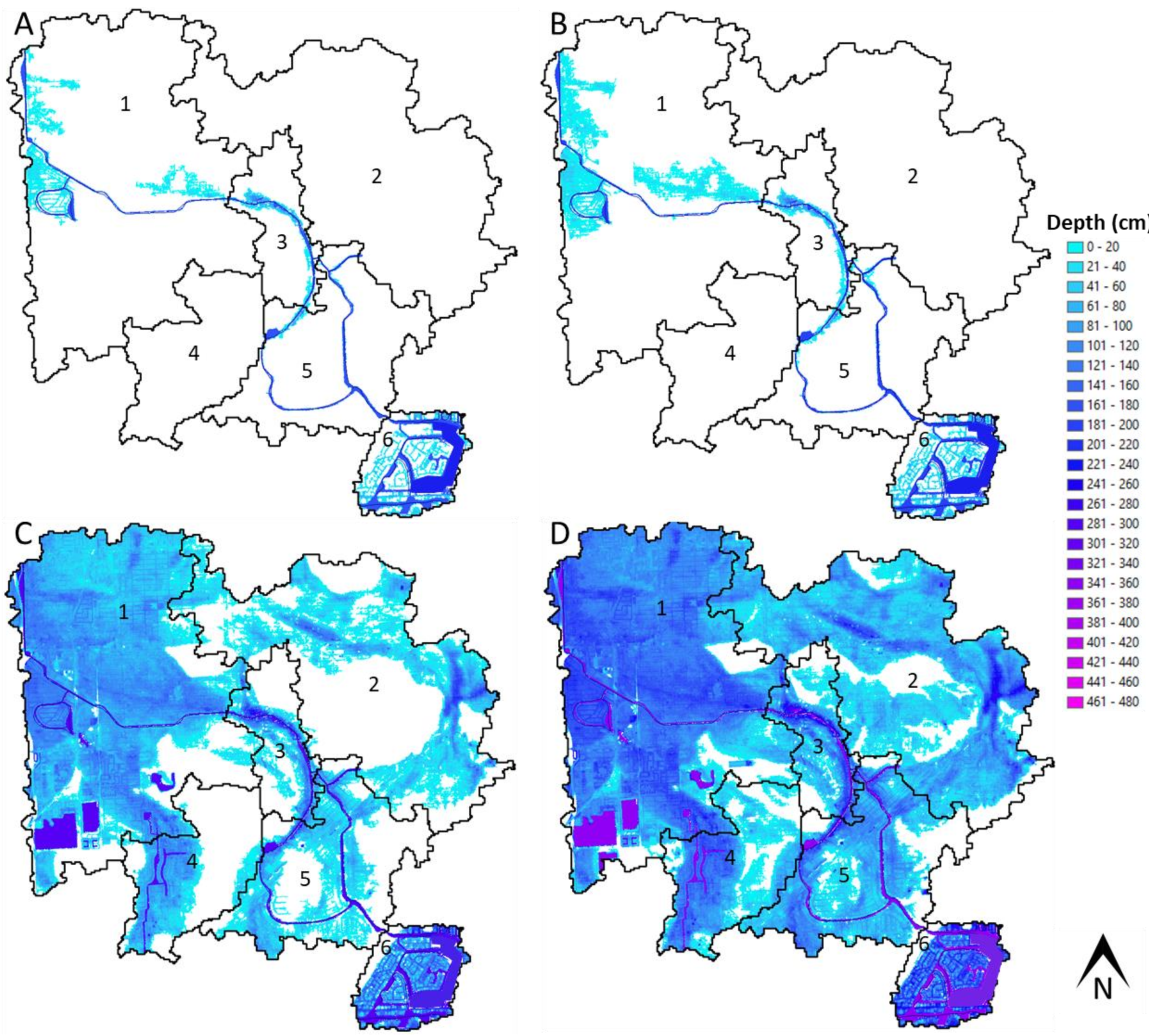

Figure 15. Sea-level rise in the Coral Gables Canal watershed, NOAA Intermediate High scenario. A) Current conditions (year 2017), B) Year 2060, C) Year 2100, D) Year 2120. Boundaries of the Coral Gables Canal watershed and sub-watershed numbers are shown.

Figure 15 shows inundation maps under NOAA Intermediate High sea-level rise scenario in the Coral Gables Canal watershed. The simulations show that there was minimal flooding during year 2017 (Irma Hurricane), mostly at areas close to the coast (sub-basin 6), around gate G93 (center of the watershed at the intersection of the canal with the boundary between sub-basins 1 and 3), and areas close to the Tamiami Canal (Northwest sector of the watershed, sub-basin 1). For year 2060 the model predicted that inundated areas would expand in sub-basins 1, 3 and 6 with water depths smaller than 1.0 m, while sub-basins 2 and 4 are not flooded (Figure 16). For year 2100, inundated areas appear at the perimetral sectors of the watershed and expand greatly in the coastal, central, and northwest sectors of the watershed (Figure 15). At least 40% of the CGC watershed is inundated with water depths greater than 0.6 m, being sub-basins 1 and 6 flooded in at least 70%, with water depths reaching 1.2 m (Figure 16). Water depths increased reaching up to 1.8 m in urban areas close to the canal.

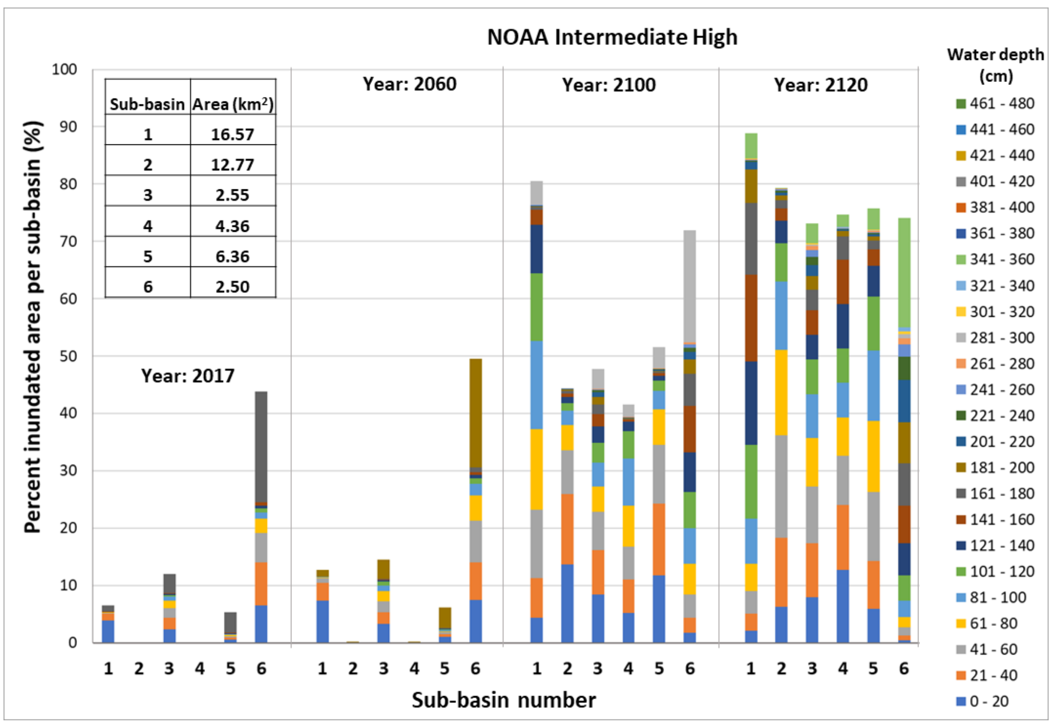

Figure 16. Percent inundated area per sub-basin in the Coral Gables Canal watershed. Total sub-basin areas (in km^2) are shown in the embedded table. The vertical axis shows percent of the sub-basin area that are inundated under NOAA Intermediate High scenario, for years 2016, 2100, and 2120. Water depth intervals shown in the legend are represented in colors for each sub-basin.

Figure 16 shows that under NOAA Intermediate High sea-level rise scenario, inundated areas in year 2120 cover at least 70% of the CGC watershed, with water depths greater than 1.6 m, reaching up to 3.4 m in urban sectors of sub-basins 1, 3, 4, 5, and 6. The model predicts that 88% of urban areas in sub-basin 1 are flooded.

A similar exploration for sea-level rise under the NOAA High scenario is presented in Figure 17. Inundation is shown to be exacerbated by the extreme rise in water elevations. For year 2060, flooded areas are similar in spatial coverage to those corresponding to NOAA Intermediate High scenario. However, the coverage of inundated areas in sub-basin 1 almost triples, increasing from 12% to 29% flooding of the total sub-basin area (Figure 18). Sub-basin 2 is shown to have minimal flooding as in the NOAA Intermediate High scenario.

The most striking results correspond to years 2100 and 2120. If an event similar to Irma hurricane would occur, the model predicted that at least 70% of the Coral Gables Canal watershed would be inundated in 2100 with water depths greater than 1.0 m (Figure 18). Water depths would reach at 1.8 m in almost 40% of the watershed area. More than 80% of the area corresponding to sub-basins 1, 2 and 4 will be inundated with water depths reaching 1.6 m.

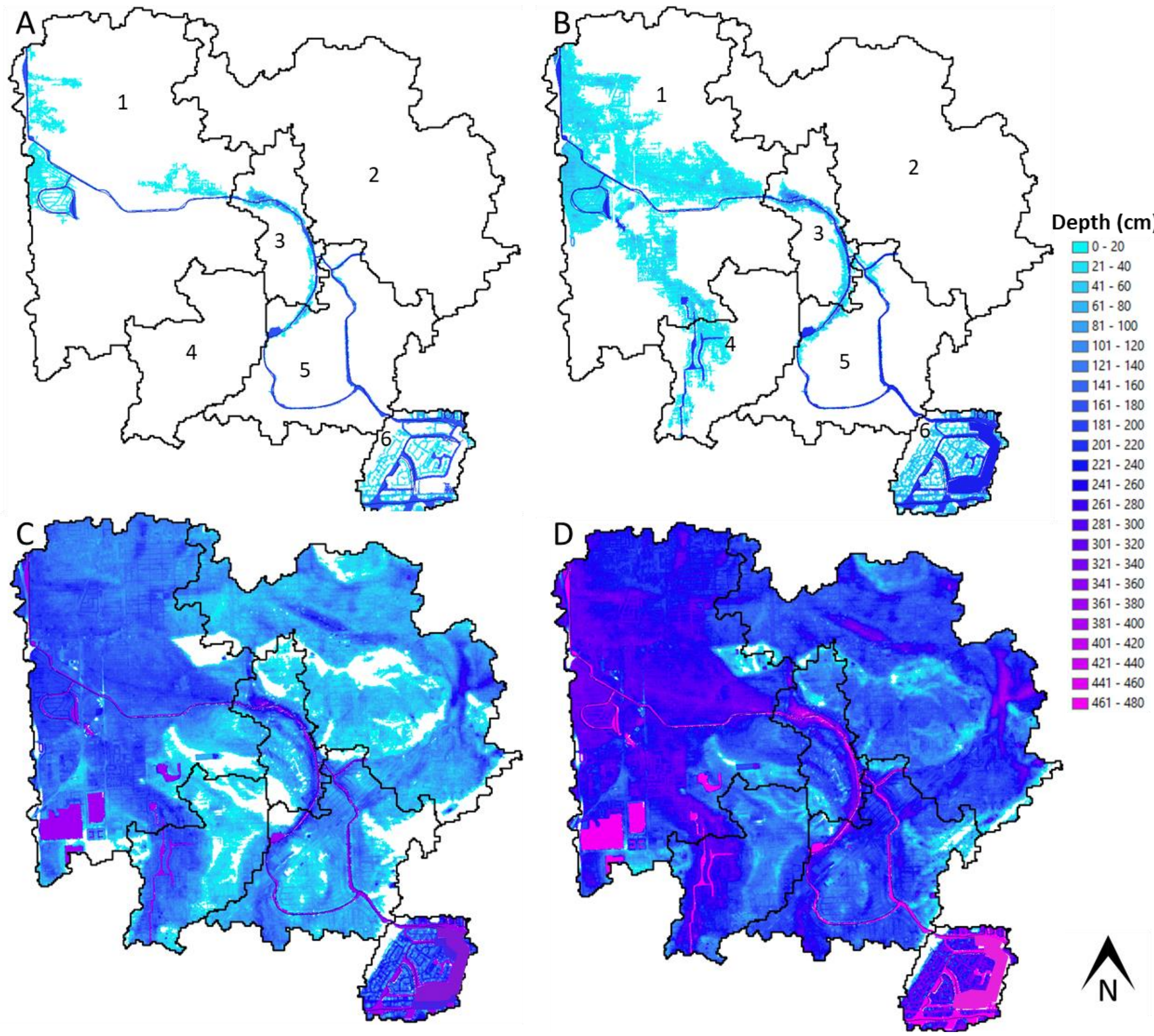

Figure 17. Sea-level rise in the Coral Gables Canal watershed, NOAA High scenario. A) Current conditions (year 2017), B) Year 2060, C) Year 2100, D) Year 2120. Boundaries of the Coral Gables Canal watershed and sub-watershed numbers are shown.

The simulation for year 2120 shows that water depths would reach between 1.8 m to 3.6 m in urban sectors surrounding the upper portion of the canal, while the rest of the watershed will be inundated by water depths between 0.6 m to 2.2 m. Sub-basins 1 through 5 will be inundated in at least 90% of their areal extent with water depths reaching up to 4.8 m.

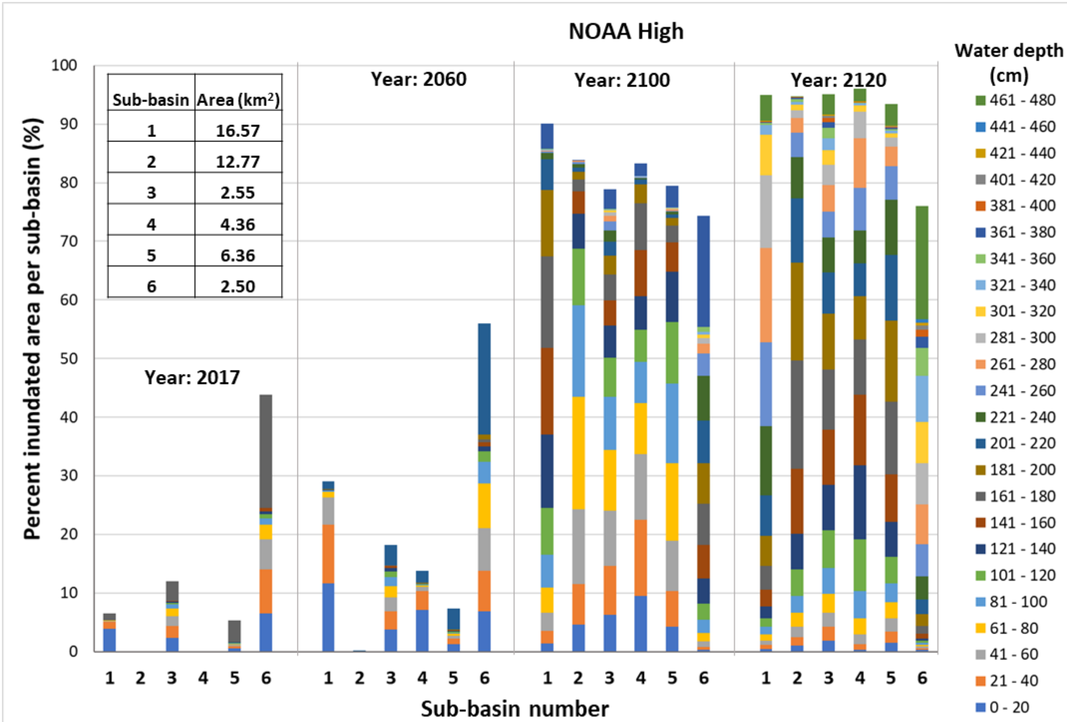

Figure 18. Percent inundated area per sub-basin in the Coral Gables Canal watershed. Total sub-basin areas (in km^2) are shown in the embedded table. The vertical axis shows percent of the sub-basin area that are inundated under NOAA High scenario, for years 2016, 2100, and 2120. Water depth intervals shown in the legend are represented in colors for each sub-basin.

4. Discussion

As shown in the previous section, the findings of this research focus on the combined effects of gradual sea level rise (SLR) and extreme events (Irma hurricane) on water surface elevations at the Coral Gables Canal (CGC), and inundation at the CGC watershed. The results show that the inundation coverage in the CGC watershed is greater by 72% to 85% than estimations made accounting only for SLR and not for extreme events. This is a consequence of underpredicting maximum water surface elevations in the Coral Gables Canal occurring under combined forcing.

The estimated WSE in this research are 16% greater than the WSE estimated in the NOAA Extreme SLR scenario, 44% greater with respect to NOAA High scenario, and 61% greater than the NOAA-Intermediate High scenario. The NOAA scenarios do not consider compounded SLR and extreme events effects on WSE and inundation at local scale. The increased WSE and inundated areas estimation presented in this paper are consistent with results published in recent international research.

Sea level rise is not globally uniform and varies regionally, therefore a consideration of local processes is critical for projections of sea level impacts at local scales (IPCC, 2019). Over the last several decades, a rapid change in the annual frequencies of tidal flooding has been documented at NOAA tide gauges along the U.S. coastline (NOAA, 2018). Mean sea level is rising worldwide, and correlated changes in ocean tides are also occurring, leading to increased coastal inundation and nuisance flooding events in sensitive regions all over the world (Devlin et al., 2019). This is because even limited changes in mean sea level will have a noticeable effect on the occurrence of extreme sea-level events (tides, surges, etc.) IPCC (2019). Climate change and sea level rise are altering the statistics of extreme events in a rather complex fashion: events that are historically rare today will become common in the future (Yin et al., 2020). For example, coastal events with return period of 100 years or larger will occur yearly by the middle of 2021 under all RPC scenarios (IPCC, 2019). Flood risk associated to individual events (that have a limited duration) should be assessed superimposed on gradual sea level rise (Almar et al., 2021).

At a global scale, Pickering et al. (2017) and Almar et al. (2021) studied the effect of future SLR on global tides and the related flood risk implications. Their findings reveal that SLR augments tidal effects posing substantially increased flood risk to coastal zones all over the world. Kulp and Strauss (2019) in an assessment of the potential exposure to extreme water levels on top of rising seas, found that previous estimates of global vulnerability to sea-level rise and coastal flooding would triple when compounded effects are considered. This is consistent with Ezer and Atkinson (2014) that showed that the U.S. East Coast is a "hotspot of accelerated flooding" due to increased occurrence of storm surges and high tide, which results in increased flood durations. Also, NOAA (2018) reports that high tide flood frequencies will continue to increase sooner where SLR rates are higher (US Western Gulf and Northeast Atlantic coasts), and where SLR rates are lower (Southeast Atlantic) high tide flood frequencies will experience the fastest rate of increase.

At regional and local scales studies performed in Europe and Asia have reported similar results. Arns et al. (2016) in a study of the effects of SLR on water surface elevations (WSE) estimations used for designing coastal defenses in the German Wadden Sea, found that SLR amplify WSE by an average of 48%–56%, relative to WSE caused by SLR alone. Arns et al. (2016) indicated that tides occurring under RCP8.5 extreme scenario (RCP8.5HE, year 2100) are amplified by 320% relative to SLR. As shown in previous sections, in this research it is estimated that during Irma hurricane WSE at the Coral Gables Canal were amplified by 50% to 400%. Similarly, Kim (2020) in an inundation study due to coupled effects of sea-level rise and surge under the future global climate change scenarios for the Korean peninsula, found that WSE increases by 50% to 250% water surface elevations estimated under SLR forcing alone. Sayol and Marcos (2018) estimated the impact of combined local sea level rise and extreme events in flooding of Spanish coastal areas (Ebro River delta), under several climate change scenarios. Sayol and Marcos (2018) found that SLR combined with extreme events increase flooded areas by 77% (under RCP4.5, year 2099), with respect to flooded areas estimated under SLR alone. For the Coral Gables Canal watershed, estimated inundation coverage calculated in this research (SLR combined with an extreme event) was 72% to 85% greater that flooding calculated with SLR alone (NOAA Intermediate High SLR scenario for year 2100).

5. Conclusions

Quantitative analysis of observed water surface elevations at the Virginia Key station (ocean boundary for the hydrodynamic mode) and G93-H/G93-T stations (located in the Coral Gables Canal, CGC) shows that water surface elevation peaks at Virginia Key are increased significatively by hydrodynamic processes. During the Irma hurricane, water surface elevations at the canal stations increased up to 0.56 m with respect to water surface elevations observed at Virginia Key station. The hydrodynamic model estimated that similar increases will be produced under sea-level rise scenarios. This result reinforces the need for local hydrodynamic estimations of water surface elevations for assessing the impacts of sea-level rise. Current estimations in the area are based on data collected at Virginia Key station and miss the increase of water levels in the CGC canal.

An exploration of the inundation consequences on Coral Gables Canal watershed if an event similar to Irma hurricane would occur under projected sea-level rise scenarios, revealed that inundation would be more severe than inundation projections produced by online sea-level rise simulators. Under NOAA Intermediate High sea-level rise scenario (year 2100) at least 40% of the CGC watershed is inundated with water depths greater than 0.6 m, reaching 1.2 m in some sectors. Inundated areas in year 2120 cover at least 70% of the CGC watershed, with water depths greater than 1.6 m, reaching up to 3.4 m in urban sectors close to the canal.

The hydrodynamic model predicted that under the NOAA High sea-level rise scenario at least 70% of the Coral Gables Canal watershed would be inundated in 2100 with water depths greater than 1.0 m. Water depths would reach 1.8 m in almost 40% of the watershed area. The simulation for year 2120 shows that water depths would reach between 1.8 m to 3.6 m in urban sectors surrounding the upper portion of the canal, while 90% of inland sub-basins will be inundated by water depths between 0.6 m to 2.2 m. Water depths in low lying areas will reach up to 4.8 m.

A comparison of flooding areas generated in this research to estimations made by several online tools shows that the inundation coverage and water depths produced by those simulators are noticeably smaller. For the NOAA Intermediate High scenario, the model calculates that the inundated area covers 27 km^2, while Surging Seas Climate Central and NOAA Sea-Level Rise viewers estimate that only 8 km^2 will be inundated. The Florida Sea-level Scenario Sketch Planning tool estimates that approximately 4 km^2 will be flooded. This is a consequence of underpredicting maximum water surface elevations in the Coral Gables Canal. The results presented in this paper show that a robust sea-level rise vulnerability assessment should be based on local estimations of the combined effect of mean and extreme sea-level rise. Besides providing a more realistic inundation spatial coverage, a detailed spatial distribution and magnitudes of water depths is presented. This could also be significant for flooding/inundation risk management decisions. Having an accurate spatial estimation of inundation coverage and water depths could contribute to better assessing high-risk of inundation for existing and planned critical infrastructure.

Recently published research has shown that extreme sea-level events will become more frequent in the future, and their potential consequences should be added to those of gradual sea-level rise when assessing flood exposure. In this context, the methodology presented in this research could contribute significantly toward the development of management measures required for providing a safety factor to potential critical projects in the Coral Gables area, and in the larger southeast Florida that has similar urban and physiographic characteristics.

Declarations

Funding: This research was funded by a NOAA/Atlantic Oceanographic and Meteorological Laboratory grant to the Northern Gulf Institute (award number NA160AR4320199).

Conflicts of interest/Competing interests: The authors declare that they have no conflict of interest.

Availability of data and material (data transparency): Data will be publicly available through NOAA/NGI data portals.

Code availability (software application or custom code): Not applicable

Ethical Approval: Not applicable.

Consent to Participate: Not applicable.

Consent to Publish: Not applicable.

Authors Contributions:

- V. J. Alarcon: Writing-original draft, formal analysis, conceptualization, modeling.
- A. C. Linhoss: Formal analysis, review, editing.
- C. R. Kelble: Formal analysis, review, editing.
- P. F. Mickle: Formal analysis, review, editing.
- G. F. Sanchez-Banda: Conceptualization, modeling.
- F. E. Mardonez-Meza: Conceptualization, modeling.
- J. Bishop: Formal analysis.
- S. L. Ashby: Review

References

Alarcon, V.J., Johnson, D., McAnally, W.H. et al. (2014). Nested Hydrodynamic Modeling of a Coastal River Applying Dynamic-Coupling. Water Resources Management, 28, 3227–3240 (2014). https://doi.org/10.1007/s11269-014-0671-6

Almar, R., Ranasinghe, R., Bergsma, E.W.J. et al. (2021). A global analysis of extreme coastal water levels with implications for potential coastal overtopping. Nat Commun 12, 3775 (2021). https://doi.org/10.1038/s41467-021-24008-9

Allen, J.I., Somerfield, P.J., Gilbert, F.J. (2007). Quantifying uncertainty in high-resolution coupled hydrodynamic-ecosystem models, Journal of Marine Systems, Volume 64, Issues 1–4, 2007, Pages 3-14, https://doi.org/10.1016/j.jmarsys.2006.02.010.

Anderson, T.R., Fletcher, C.H., Barbee, M.M. et al. (2018). Modeling multiple sea level rise stresses reveals up to twice the land at risk compared to strictly passive flooding methods. Sci Rep 8, 14484 (2018). https://doi.org/10.1038/s41598-018-32658-x

Arns, A., Dangendorf, S., Jensen, J. et al. (2017). Sea-level rise induced amplification of coastal protection design heights. Sci Rep 7, 40171 (2017). https://doi.org/10.1038/srep40171

Aucan, J. (2018). Effects of Climate Change on Sea Levels and Inundation Relevant to the Pacific Islands. Science Review 2018: pp 43-49. https://reliefweb.int/sites/reliefweb.int/files/resources/4_Sea_Level_and_Inundation.pdf

Bouck, D. L. (2017). Determining trends in water quality using high resolution land use data. Master's Thesis. University of Miami, 2017.

Caccia VG, Boyer JN. (2007). A nutrient loading budget for Biscayne Bay, Florida. Mar Pollut Bull. 2007 Jul;54(7):994-1008. Epub 2007 Apr 5. PMID: 17418240. https://doi.org/10.1016/j.marpolbul.2007.02.009

Cazenave, A. and Le Cozannet, G. (2014). Sea level rise and its coastal impacts. Earth's Future. 2. 15-34. https://doi.org/.1002/2013EF000188

Climate Central (2021). Surging Seas Risk Zone Map. https://sealevel.climatecentral.org/

Devlin, A.T., Pan, J., Lin, H. (2019). Tidal variability in the Hong Kong region. (2019) Ocean Science, 15 (4), pp. 853-864. https://doi.org/10.5194/os-15-853-2019

Ezer, T. and Atkinson, L.P. (2014), Accelerated flooding along the U.S. East Coast: On the impact of sea-level rise, tides, storms, the Gulf Stream, and the North Atlantic Oscillations. Earth's Future, 2: 362-382. https://doi-org.sibudp.idm.oclc.org/10.1002/2014EF000252

Fu, X., Nijman, J. (2021). Sea Level Rise, Homeownership, and Residential Real Estate Markets in South Florida (2021). Professional Geographer, 73 (1), pp. 62-71. https://doi.org/10.1080/00330124.2020.1818586

Gornitz, V., Rosenzweig, C., Hillel, D. (1997). Effects of anthropogenic intervention in the land hydrologic cycle on global sea level rise. Global and Planetary Change, Volume 14, Issues 3–4, 1997, Pages 147-161, https://doi.org/10.1016/S0921-8181(96)00008-2

Hall, J.A., S. Gill, J. Obeysekera, et al. (2016). Regional Sea Level Scenarios for Coastal Risk Management: Managing the Uncertainty of Future Sea Level Change and Extreme Water Levels for Department of Defense Coastal Sites Worldwide. U.S. Department of Defense, Strategic Environmental Research and Development Program. 224 pp. https://climateandsecurity.files.wordpress.com/2014/01/regional-sea-level-scenarios-for-coastal-risk-management_managing-uncertainty-of-future-sea-level-change-and-extreme-water-levels-for-department-of-defense.pdf

Hamrick J. M., 1992. A three-dimensional environmental fluid dynamics computer code: theoretical and computational aspects. Special Report 317 in Applied Marine Science and Ocean Engineering. The College of William and Mary, Virginia Institute of Marine Science. 63 pp.

IPCC, 2019. IPCC Chapter 4: Sea Level Rise and Implications for Low-Lying Islands, Coasts and Communities. https://www.ipcc.ch/srocc/chapter/chapter-4-sea-level-rise-and-implications-for-low-lying-islands-coasts-and-communities/

Jane, R., Cadavid, L., Obeysekera, J., and Wahl, T. (2020). Multivariate statistical modelling of the drivers of compound flood events in south Florida. Nat. Hazards Earth Syst. Sci., 20, 2681–2699, 2020. https://doi.org/10.5194/nhess-20-2681-2020

Jevrejeva, S., Grinsted, A., and Moore, J. C. (2009), Anthropogenic forcing dominates sea level rise since 1850, Geophys. Res. Lett., 36, L20706, https://doi.org/10.1029/2009GL040216

Jones, M.C., Wingard, G.L., Stackhouse, B., Keller, K., Willard, D., Marot, M., Landacre, B., E. Bernhardt, C. (2019). Rapid inundation of southern Florida coastline despite low relative sea-level rise rates during the late-Holocene (2019) Nature Communications, 10 (1), art. no. 3231. https://doi.org/10.1038/s41467-019-11138-4

Kim, Y.H. (2020). Assessment of Coastal Inundation due to Storm Surge under Future Sea-Level Rise Conditions. (2020) Journal of Coastal Research, 95 (sp1), pp. 845-849. https://doi.org/10.2112/SI95-164.1

Knoben, W. J. M., Freer, J. E., Woods, R. A. (2019). Technical note: Inherent benchmark or not? Comparing Nash–Sutcliffe and Kling–Gupta efficiency scores. Hydrol. Earth Syst. Sci., 23, 4323–4331, 2019. https://doi.org/10.5194/hess-23-4323-2019

Kulp, S.A., Strauss, B.H. (2019). New elevation data triple estimates of global vulnerability to sea-level rise and coastal flooding. Nat Commun 10, 4844 (2019). https://doi.org/10.1038/s41467-019-12808-z

Lang, A., Mikolajewicz, U. (2020). Rising extreme sea levels in the German Bight under enhanced CO2 levels: a regionalized large ensemble approach for the North Sea. Clim Dyn 55, 1829–1842 (2020). https://doi.org/10.1007/s00382-020-05357-5

Millette, N.C., Kelble, C., Linhoss, A., Ashby, S., Visser, L., 2019. Using Spatial Variability in the Rate of Change of Chlorophyll a to Improve Water Quality Management in a Subtropical Oligotrophic Estuary (2019). Estuaries and Coasts, 42 (7), pp. 1792-1803. https://doi.org/10.1007/s12237-019-00610-5

Moriasi, D.N., Arnold, J.G., Van Liew, M.W., Bingner, R.L., Harmel, R.D., Veith, T.L. (2007). Model Evaluation Guidelines for Systematic Quantification of Accuracy in Watershed Simulations. Trans. ASABE 2007, 50, 885–900, https://doi.org/10.13031/2013.23153

Neuman, T. and Ahrendt, K. (2013). Comparing the "Bathtub Method" with MIKE21 HD flow model for modelling storm surge inundation - Case study Kiel Fjord. Thesis, Geographisches Institut, Universität Kiel.
https://edoc.sub.uni-hamburg.de/klimawandel/files/835/RADOST_BATHTUB_034.pdf

NOAA National Oceanic and Atmospheric Administration (2021). Sea Level Rise Viewer. https://coast.noaa.gov/slr/#

NOAA, National Oceanic and Atmospheric Administration (2020). Tides & Currents. https://tidesandcurrents.noaa.gov/stationhome.html?id=8723214

NOAA, , National Oceanic and Atmospheric Administration 2018. Patterns and Projections of High Tide Flooding Along The U.S. Coastline Using a Common Impact Threshold. https://tidesandcurrents.noaa.gov/publications/techrpt86_PaP_of_HTFlooding.pdf

NOAA, National Oceanic and Atmospheric Administration (2017a). Digital Coast: Sea Level Rise Viewer. https://coast.noaa.gov/data/digitalcoast/pdf/slr-faq.pdf

NOAA Office for Coastal Management (2017b). Digital Coast Sea Level Rise Viewer: Frequent Questions. https://coast.noaa.gov/data/digitalcoast/pdf/slr-faq.pdf

NOAA (2017c). Global and regional sea level rise scenarios for the United States. Center for Operational Oceanographic Products and Services. NOAA Technical Report NOS CO-OPS 083. https://tidesandcurrents.noaa.gov/publications/techrpt83_Global_and_Regional_SLR_Scenarios_for_the_US_final.pdf

NOAA/NOS (2020). Biscayne Bay (S200) Bathymetric Digital Elevation Model - NOAA/NOS Estuarine Bathymetry. https://data.noaa.gov/dataset/dataset/biscayne-bay-s200-bathymetric-digital-elevation-model-noaa-nos-estuarine-bathymetry

NOAA Coastal Service Center (2010). Mapping Inundation Uncertainty. https://coast.noaa.gov/data/digitalcoast/pdf/mapping-inundation-uncertainty.pdf

Palm, R., Bolsen, T. (2020). The Science of Climate Change and Sea-Level Rise

(2020). Coastal Research Library, 34, pp. 5-13. https://doi.org/10.1007/978-3-030-32602-9_2

Oppenheimer, M., Glavovic, B.C., Hinkel, J. et al. (2019). Sea Level Rise and Implications for Low-Lying Islands, Coasts and Communities. In: IPCC Special Report on the Ocean and Cryosphere in a Changing Climate [Pörtner, H. O., Roberts, D.C., Masson-Delmotte, V. et al. (eds.)]. https://www.ipcc.ch/srocc/chapter/chapter-4-sea-level-rise-and-implications-for-low-lying-islands-coasts-and-communities/

Pednekar G. and Siva Raju S. (2020). Sea Level Rise and Its Socio-economic Impacts: A Case Study in Mumbai, India. In: Akhtar R. (eds) Extreme Weather Events and Human Health. Springer, Cham. https://doi.org/10.1007/978-3-030-23773-8_11

Pickering, M.D., K.J. Horsburgh, J.R. Blundell, J.J.-M. Hirschi, R.J. Nicholls, M. Verlaan, N.C. Wells (2017). The impact of future sea-level rise on the global tides. Continental Shelf Research, Volume 142, 2017, pp 50-68. https://doi.org/10.1016/j.csr.2017.02.004

Sallenger, A. H. Jr., Doran, K. S., and Howard, P. A. (2012). Hotspot of accelerated sea-level rise on the Atlantic coast of North America. Nat. Clim. Chang. 2, 884–888. https://doi.org/10.1038/nclimate1597

Santos, R.O., Lirman, D., Pittman, S.J., Serafy, J.E. (2018). Spatial patterns of seagrasses and salinity regimes interact to structure marine faunal assemblages in a subtropical bay. (2018) Marine Ecology Progress Series, 594, pp. 21-38. https://doi.org/10.3354/meps12499

Sayol, J.M., Marcos, M. (2018). Assessing Flood Risk Under Sea Level Rise and Extreme Sea Levels Scenarios: Application to the Ebro Delta (Spain). (2018) Journal of Geophysical Research: Oceans, 123 (2), pp. 794-811. https://doi.org/10.1002/2017JC013355

SFRCCC, Southeast Florida Regional Climate Change Compact Sea Level Rise Work Group (Compact) (2020). Unified Sea Level Rise Projection Southeast Florida. A document prepared for the Southeast Florida Regional Climate Change Compact Climate Leadership Committee. 36p. https://southeastfloridaclimatecompact.org/unified-sea-level-rise-projections/

SFWMD, South Florida Water Management District (2020). DBHYDRO (Environmental Data). https://www.sfwmd.gov/science-data/dbhydro

Singh, R. K., Villuri, V. G. K., Pasupuleti, S., Nune, R. (2020). Hydrodynamic modeling for identifying flood vulnerability zones in lower Damodar river of eastern India. Ain Shams Engineering Journal, Volume 11, Issue 4, 2020, Pages 1035-1046. https://doi.org/10.1016/j.asej.2020.01.011

Slangen, A., Church, J., Agosta, C. et al. (2016). Anthropogenic forcing dominates global mean sea-level rise since 1970. Nature Clim Change 6, 701–705 (2016). https://doi.org/10.1038/nclimate2991

Swart, P.K., Anderson, W.T., Altabet, M.A., Drayer, C. and Bellmund, S. (2013). Sources of dissolved inorganic nitrogen in a coastal lagoon adjacent to a major metropolitan area, Miami Florida (USA). Applied Geochemistry, 38, 134-146.

Sweet, W.V., Kopp, R.E., Weaver, C.P., Obeysekera, J., Horton, R.M., Thieler, E.R., & Zervas, C. (2017). Global and Regional Sea Level Rise Scenarios for the United States. NOAA Technical report NOS CO-OPS 083, Silver Spring, Md., 75 p.

Tetratech, Inc. (2007). The Environmental Fluid Dynamics Code: Theory and Computation, Volume 2: Sediment and Contaminant Transport and Fate, Fairfax, VA. http://www.tetoc.com/file?id=402880ec3f433ae8013f4354145d000a

University of Florida (2021). GeoPlan Center: Florida Sea Level Scenario Sketch Planning Tool. https://sls.geoplan.ufl.edu/viewer/

Vitousek, S., P. L. Barnard, C. H. Fletcher, N. Frazer, L. Erikson, and C. D. Storlazzi (2017). Doubling of coastal flooding frequency within decades due to sea-level rise, Sci. Rep., 7 (1), 1399, https://doi.org/10.1038/s41598-017-01362-7

Wingard, G.L. (2021). Climate, Sea Level, and People – Changing South Florida's Mangrove Coast (2021) Springer Climate, pp. 189-211. https://doi.org/10.1007/978-3-030-52383-1_12

Yin, J., Griffies, S.M., Winton, M., Zhao, M., Zanna, L. (2020). Response of storm-related extreme sea level along the U.S. Atlantic coast to combined weather and climate forcing (2020) Journal of Climate, 33 (9), pp. 3745-3769. https://doi.org/10.1175/JCLI-D-19-0551.1

Yunus, A.P., Avtar, R., Kraines, S., Yamamuro, M., Lindberg, F., Grimmond, C.S.B. (2016). Uncertainties in Tidally Adjusted Estimates of Sea Level Rise Flooding (Bathtub Model) for the Greater London. Remote Sens. 2016, 8, 366. https://doi.org/10.3390/rs8050366